The ISME Journal (2015), 1–13

www.nature.com/ismej

ORIGINAL ARTICLE

Structure and function of natural sulphide-oxidizing microbial mats under dynamic input of light and chemical energy

Judith M Klatt[1], Steffi Meyer[1], Stefan Häusler[1], Jennifer L Macalady[2], Dirk de Beer[1] and Lubos Polerecky[1,3]

[1]*Microsensor Research Group, Max Planck Institute for Marine Microbiology, Bremen, Germany;* [2]*Pennsylvania State University, University Park, State College, PA, USA and* [3]*Department of Earth Sciences—Geochemistry, Faculty of Geosciences, Utrecht University, Utrecht, The Netherlands*

We studied the interaction between phototrophic and chemolithoautotrophic sulphide-oxidizing microorganisms in natural microbial mats forming in sulphidic streams. The structure of these mats varied between two end-members: one characterized by a layer dominated by large sulphur-oxidizing bacteria (SOB; mostly *Beggiatoa*-like) on top of a cyanobacterial layer (B/C mats) and the other with an inverted structure (C/B mats). C/B mats formed where the availability of oxygen from the water column was limited (<5 μM). Aerobic chemolithotrophic activity of the SOB depended entirely on oxygen produced locally by cyanobacteria during high light conditions. In contrast, B/C mats formed at locations where oxygen in the water column was comparatively abundant (>45 μM) and continuously present. Here SOB were independent of the photosynthetic activity of cyanobacteria and outcompeted the cyanobacteria in the uppermost layer of the mat where energy sources for both functional groups were concentrated. Outcompetition of photosynthetic microbes in the presence of light was facilitated by the decoupling of aerobic chemolithotrophy and oxygenic phototrophy. Remarkably, the B/C mats conserved much less energy than the C/B mats, although similar amounts of light and chemical energy were available. Thus ecosystems do not necessarily develop towards optimal energy usage. Our data suggest that, when two independent sources of energy are available, the structure and activity of microbial communities is primarily determined by the continuous rather than the intermittent energy source, even if the time-integrated energy flux of the intermittent energy source is greater.

The ISME Journal advance online publication, 25 September 2015; doi:10.1038/ismej.2015.167

Introduction

Life is driven by essentially two types of energy: chemical energy, in the form of chemical disequilibria, and physical energy carried by light of suitable wavelengths. On geological timescales, changes in energy fluxes and the development of new strategies of life are closely coupled. One of the most important changes in energy availability was the evolution and proliferation of oxygenic photosynthesis. The onset of this process introduced the thermodynamically most favourable electron-acceptor oxygen to the wider reduced environment. Oxygenic photosynthesis therefore provided previously unexplored thermodynamic disequilibria to other microorganisms thereby allowing for the evolution and diversification of aerobic metabolisms (Castresana and Saraste, 1995; Dismukes *et al*., 2001; Catling *et al*., 2005).

Insights into the revolutionary milestones associated with the evolution and proliferation of oxygenic photosynthesis can be gained by studying modern model ecosystems in environments whose geochemical/energetic characteristics exhibit spatial gradients that are analogous to the temporal transition from a reduced to an oxidized state of the Earth's surface. The thin microbial mats forming at the bottom of light-exposed cold sulphidic springs at Frasassi, Italy, (Galdenzi *et al*., 2008) are such an analogue system as they are distributed across a gradient from reduced to oxidized conditions in the overlying water column. These contemporary phototrophic microbial mats are of particular interest as they represent analogues to ancient cyanobacterial mats (for example, stromatolites) that are thought to have been extensive in shallow waters throughout the Proterozoic and possibly already in the Archean (Ward *et al*., 1992; Grotzinger and Knoll, 1999; Allwood *et al*., 2009; Seckbach and Oren, 2010; Schopf, 2012).

Correspondence: JM Klatt or L Polerecky, Microsensor Research Group, Max Planck Institute for Marine Microbiology, Celsiusstrasse 1, Bremen 28359, Germany.
E-mail: jklatt@mpi-bremen.de or l.polerecky@uu.nl
Received 19 January 2015; revised 8 August 2015; accepted 12 August 2015

In this study, we used microsensors to quantify energy fluxes available for and conserved by the dominant processes in the mats—photosynthesis (P) and aerobic sulphide oxidation (SO)—with the aim to understand how the interaction between these processes under a fluctuating input of chemical and light energy determines the structure and function of the mats. We hypothesized that under the different conditions the mats develop towards a system that conserves the available energy optimally. We discuss the important role of energy dynamics on microbial mat structure and possible implications of our results in the context of Earth's oxygenation.

Materials and methods

Study site
This study was performed in streams and pools where the sulphidic waters from the Frasassi Cave system in the Frasassi Gorge, Italy, emerge and mix with waters of the Sentino river (Galdenzi *et al*., 2008). The study sites included the outflows of two perennial springs, the Fissure Spring and the Main Spring (43°24′4″N, 12°57′56″E).

Water chemistry
Sampling for bulk water chemistry analysis was carried out in May and September 2009 and in September 2012. Samples were taken during night and around midday within a few cm above the microbial mat patches and were preserved immediately in gas-tight vials containing a mixture of 100 µl of 20% $ZnCl_2$ and 50 µl of saturated $HgCl_2$ solution. The vials were filled with water samples until there was no head space and kept at room temperature until quantification in Bremen. Dissolved inorganic carbon and ammonium were determined using flow injection analysis (Hall and Aller, 1992). The sum of nitrate and nitrite was quantified according to Braman and Hendrix (1989) using an NOx analyser equipped with a chemiluminescence detector (Model CLD 66, Eco Physics, Dürnten, Switzerland). pH and concentrations of dissolved O_2 and total sulphide ($S_{tot} = [S^{2-}]+[HS^-]+[H_2S]$) were determined with microsensors. Temperature at the mat surface was measured with a PT1000 mini-sensor (Umweltsensortechnik, Geschwenda, Germany).

Microscopy
The dominant members of the mat community were identified by microscopy. Imaging by bright field, phase contrast and fluorescence microscopy was carried out using an Axiophot epifluorescence microscope (Zeiss, Jena, Germany). Photopigments were identified on a single-cell level by hyperspectral imaging (Polerecky *et al*., 2009).

Microsensors
O_2, pH and H_2S microsensors with a tip diameter of 10–80 µm and response time of <1 s were built, calibrated and used as described previously (Revsbech, 1989; Jeroschewski *et al*., 1996; de Beer *et al*., 1997). Calibration of the H_2S microsensors was performed in acidified spring water ($pH<2$) to which NaS_2 was added stepwise. The total sulphide concentrations, S_{tot}, in the calibration solutions were determined according to Cline (1969). Calculation of S_{tot} from the local H_2S concentrations and pH values measured with microsensors was carried out according to Millero (1986), using the pK_1 value of 7.14–7.17 depending on temperature (Jeroschewski *et al*., 1996; Wieland and Kühl, 2000).

In situ microsensor and light measurements over a diel cycle
In situ measurements of O_2, pH and H_2S in the mats were carried out using previously described microsensor setups (Weber *et al*., 2007, www.microsen-wiki.net). Parallel O_2, pH and H_2S profiles were measured under naturally variable light conditions by measuring continuously over a complete diel cycle on a cloudless day.

In parallel to microsensor measurements, downwelling irradiance of the photosynthetically available radiation was recorded using a calibrated light logger (Odyssey Dataflow Systems, Christchurch, New Zealand) or a calibrated scalar irradiance microprobe (Lassen *et al*., 1992) placed next to the microsensors. The irradiance microprobe was additionally used to quantify reflectance of the mats, as previously described (Al-Najjar *et al*., 2010).

Microsensor measurements under controlled light conditions
Measurements under controlled light conditions were performed both *in situ* and *ex situ*. *In situ*, we first measured steady-state profiles of O_2, H_2S and pH in the dark and at an incident irradiance of 650 µmol photons $m^{-2} s^{-1}$ generated by a halogen lamp (KL1500, Schott, Müllheim, Germany) corresponding to the natural illumination around midday. Subsequently, volumetric rates of gross oxygenic P were determined using the O_2 microsensor-based light–dark shift method of Revsbech and Jørgensen (1983). Finally, the same light–dark shift approach was applied using H_2S and pH microsensors instead of a O_2 microsensor, which allowed quantification of volumetric rates of gross anoxygenic P in terms of consumed S_{tot} (Klatt *et al*., 2015). For this measurement, the light was switched on and off over a few minute intervals while the signals were recorded in 0.3-s intervals. All of these measurements were carried out in the same spot of the mat.

To confirm that the cyanobacterial population in the mats was able to perform simultaneous oxygenic and anoxygenic P, similar measurements were

performed *ex situ*. The mat sample was placed in a temperature-controlled (15 °C) flow chamber, and O_2, H_2S and pH were measured in parallel in the same spot of the mat under variable illumination from the halogen lamp. To assess the potential role of obligate anoxygenic phototrophs that can use light in the near infrared part of the spectrum and H_2S as the electron donor for anoxygenic P, similar measurements were additionally performed using near infrared light-emitting diodes (maximal emission at $\lambda_{max} = 740$ and 810 nm; H2A1 series, Roithner-Lasertechnik, Vienna, Austria). The measurements with and without the additional near infrared light were carried out before and after the addition of 5 μM of DCMU (3-(3,4-dichlorophenyl)-1,1-dimethylurea; Aldrich, Seelze, Germany), a specific inhibitor of oxygenic P.

Calculation of fluxes and daily energy budgets

Diffusive fluxes of O_2 and S_{tot} were calculated from the measured concentration gradients multiplied by the corresponding diffusion coefficients and factors correcting for the azimuthal angle at which the profiles were measured (Berg *et al*., 1998; Polerecky *et al*., 2007). Diffusion coefficients, *D*, were corrected for temperature, salinity and, in case of S_{tot}, for the composition of the total sulphide pool as previously described (Sherwood *et al*., 1991; Wieland and Kühl, 2000). Specifically, diffusion coefficients were $1.78 \times 10^{-5}\,cm^2\,s^{-1}$ for O_2 and $1.35 \times 10^{-5}\,cm^2\,s^{-1}$ for S_{tot}, varying by $\leqslant 3\%$ depending on the temperature in each particular measurement.

Fluxes of incident light energy were estimated from the measured downwelling irradiance, assuming that the average energy content of photons of photosynthetically available radiation is 217.5 kJ (mol photons)$^{-1}$ (Al-Najjar *et al*., 2010). The fraction of the incident light energy absorbed by the cyanobacterial population in the mats was estimated from the measured reflectance of the mats (see Supplementary Information 1).

Fluxes of energy conserved by oxygenic and anoxygenic P as well as by aerobic SO were estimated by multiplying the estimated CO_2 fluxes with the molar energy required for CO_2 fixation by the respective process. For oxygenic and anoxygenic P, the CO_2 flux was estimated from the measured fluxes of O_2 produced and S_{tot} consumed in the photosynthetically active zone assuming the stoichiometry of $O_2/CO_2 = 1$ and $S_{tot}/CO_2 = 2$, respectively. For CO_2 fixation coupled to aerobic SO, we employed the approach of Klatt and Polerecky (2015), which allows the prediction of the complete stoichiometry of autotrophic SO based on the measured S_{tot}/O_2 flux ratios. Prerequisite for these calculations is the relationship between the S^0/SO_4^{2-} production ratio and the energy conservation efficiency, that is, the ratio between the energy demand for CO_2 reduction and the energy available from O_2 reduction. To derive this relationship, we made two main assumptions: (i) When SO is in a steady state, sulphide is oxidized completely to SO_4^{2-} (Jørgensen *et al*., 2010); (ii) When the S_{tot}/O_2 consumption ratio in the SO layer varies strongly over a diel cycle, the highest measured S_{tot}/O_2 consumption ratio occurs when sulphide is oxidized incompletely to S^0, whereas the lowest measured S_{tot}/O_2 consumption ratio corresponds to complete sulphide oxidation to SO_4^{2-}. These assumptions enabled us to determine the energy conservation efficiency as a function of the S^0/SO_4^{2-} production ratio, based on which we estimated the fluxes of CO_2, energy gained and energy conserved by SO from the measured fluxes of S_{tot} and O_2 at different times during the diel cycle. Details of the CO_2 and energy flux calculations are given in Supplementary Information 2.

Daily budgets were calculated by integrating the instantaneous fluxes over the 24-h period for all relevant reactants and energy-harvesting processes involved.

Results

Mat structure vs chemical composition of the spring water

The light-exposed microbial mats from the Frasassi sulphidic springs are dominated by two functional groups: cyanobacteria, identified by the presence of the characteristic cyanobacterial pigments chlorophyll *a* and phycocyanin in the cells revealed by hyperspectral microscopy (Supplementary Figure S1), and large *Beggiatoa*-like sulphur-oxidizing bacteria (SOB; filamentous, containing sulphur inclusions, motile through gliding) (Figures 1a and b). Inferring from microscopy, hyperspectral imaging and reflectance measurements of the mats (Supplementary Figure S2), the abundance of phototrophs other than cyanobacteria was not significant in the studied mat layers.

A close inspection revealed that the structure of the mats fell essentially between two end-members: mats with a distinct cyanobacterial layer on top of a distinct SOB layer (Figure 1c), and mats with SOB on top of cyanobacteria (Figure 1d). These two mat types are hereafter referred to as C/B and B/C mats, respectively.

In the spring outflow streams, the distribution of these two mat types was patchy and varied on a centimetre to decimetre scale. Water chemistry and light measurements revealed that the physicochemical parameters directly above the mats also changed at this scale. This was mainly due to mixing of the spring water with the freshwater from the Sentino river under highly spatially variable flow conditions, which lead, for instance, to the formation of stagnant anoxic pools next to an aerated water column. The formation of a certain mat type did not correlate with the daily light dose, with temperature, pH, nitrate, ammonium, dissolved inorganic carbon, H_2S or S_{tot} concentrations in the water column

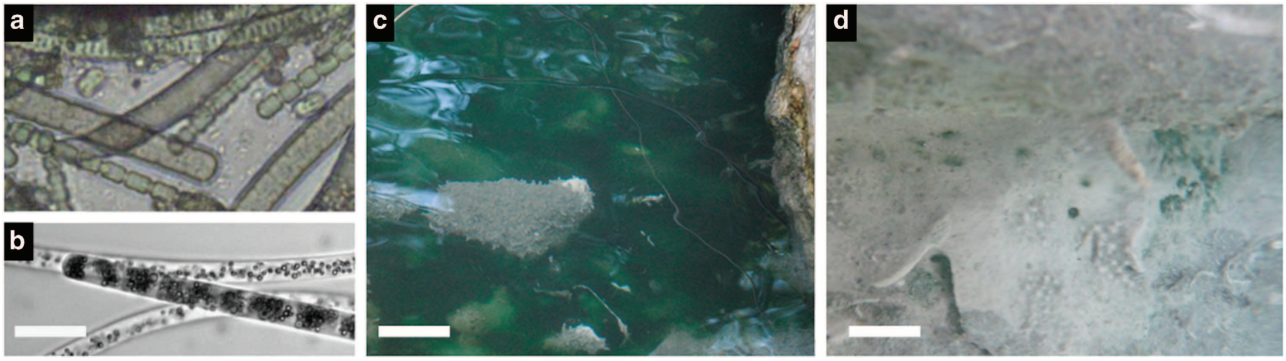

Figure 1 Microscopic images of the dominant cyanobacterial (**a**) and SOB (**b**) morphotypes in sulphide-oxidizing microbial mats from the light-exposed sulphidic streams in Frasassi, Italy, and photographs of end-member mat structures (**c**: C/B mat; **d**: B/C mat) (scale bars: **a–b**: 10 μM, **c**: 20 cm. **d**: 5 cm).

during day and night nor with the maximum H_2S and S_{tot} concentrations measured inside the mat (Table 1 and Supplementary Table S1). However, the locations harbouring the two end-member mat types clearly differed with respect to the dissolved O_2 concentration in the water column above the mats, with the C/B and B/C mats exclusively found in areas where the O_2 concentration during the night was <5 μM and >45 μM, respectively (Table 1). Changes in the water column O_2 concentration during the day, which occurred owing to the high rates of oxygenic P in the mats when the overlying water column was stagnant, had no effect on the formation of a certain mat type (compare data for mats C/B-1 and C/B-2 in Supplementary Figure S3 and Supplementary Table S1).

Photosynthetic activity of the cyanobacterial community

Laboratory microsensor measurements revealed light-induced production of O_2 and consumption of H_2S in the cyanobacterial layer of C/B (Figure 2) and B/C mats (data not shown). Although O_2 production was due to oxygenic P, removal of H_2S could be caused by three processes: chemical or biologically mediated oxidation with the photosynthetically produced O_2, a shift in the equilibrium of sulphide speciation (H_2S, HS^- and S^{2-}) induced by a pH increase associated with the uptake of dissolved inorganic carbon by oxygenic P, or by anoxygenic P that uses H_2S as the electron donor. First, H_2S oxidation with O_2 could be excluded because the H_2S dynamics changed abruptly upon light–dark transitions and were independent of O_2 concentrations. Additionally, the depth-integrated rate of gross oxygenic P matched the net rate derived from steady-state diffusive profiles (see below), showing that there is negligible oxygen reduction activity (such as owing to the reaction with H_2S) in the photosynthetically active layer. Second, assuming that total sulphide concentrations, S_{tot}, stayed constant during the light–dark transitions and pH varied as measured (by about 0.005 pH units; Figure 2), the calculated variation in H_2S would be about 1–2 orders of magnitude lower than measured (data not shown). Therefore, we exclude also the second possibility and conclude that the measured light-induced variation in H_2S was a direct result of anoxygenic P in the cyanobacterial layer of the mat.

This conclusion was confirmed by *ex situ* measurements in a C/B mat treated with DCMU, a specific inhibitor of oxygenic P but not of anoxygenic P. Specifically, H_2S concentrations in the DCMU-treated mat decreased and increased upon the addition and removal of light, respectively, while the effect on pH was marginal (data not shown) and O_2 was below detection limit (Figure 3a). For the incident irradiance of 100 μmol photons $m^{-2}\,s^{-1}$, the volumetric rates of anoxygenic P derived from light–dark shift microsensor measurements ranged between 1 and 4 mmol $S_{tot}\,m^{-3}\,s^{-1}$ (Figure 3b), and their depth-integrated value (1.53 μmol $S_{tot}\,m^{-2}\,s^{-1}$) closely matched the flux of S_{tot} removed by the cyanobacterial anoxygenic P derived from the steady-state microprofiles (1.55 μmol $S_{tot}\,m^{-2}\,s^{-1}$). This implies that anoxygenic P was the only significant sink of sulphide in the cyanobacterial layer.

The observed light-induced variability of S_{tot} could also be due to the activity of obligate anoxygenic phototrophs. The activity of such phototrophs is, however, expected to be affected by the local oxygen concentration. For example, filamentous anoxygenic phototrophs (also known as green non-sulphur bacteria) can switch from sulphide-driven anoxygenic P to photoorganoheterotrophy or aerobic respiration when oxygen and cyanobacterial excudates are available in the light (Van der Meer *et al.*, 2005; Polerecky *et al.*, 2007). Additionally, anaerobic anoxygenic phototrophs, such as green and purple sulphur bacteria, are expected to be poisoned by high oxygen concentrations (Van Gemerden and Mas, 1995). In our measurements, however, the net and gross rates of anoxygenic P before the addition of DCMU to the mat sample, that is, in the presence of oxygenic P, were almost equal to those measured after inhibition of oxygenic P by

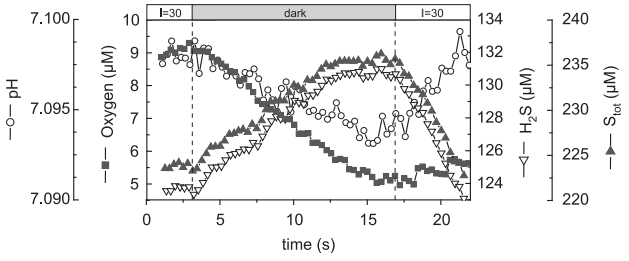

Figure 2 Light-induced dynamics of O_2, H_2S, S_{tot} and pH inside the cyanobacterial layer of a freshly collected C/B mat. Total sulphide concentrations, S_{tot}, were calculated from the measured H_2S concentrations and pH. The incident irradiance was 30 µmol photons m^{-2} s^{-1}. Distance between sensor tips was about 5 mm.

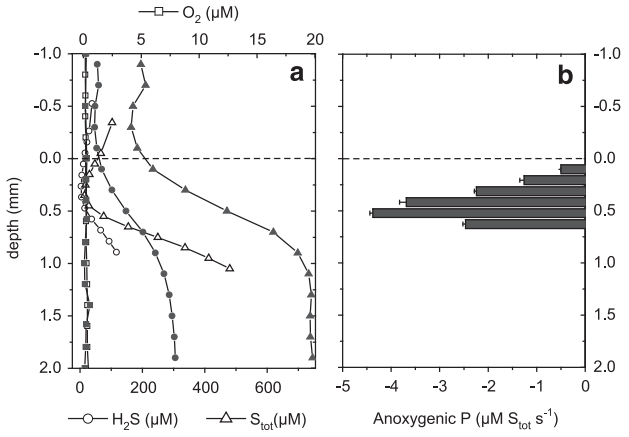

Figure 3 *Ex situ* microsensor measurements in a C/B mat after the addition of DCMU. (**a**) Steady-state depth profiles of O_2 and H_2S and S_{tot} measured in the light (open symbols) and in the dark (filled symbols). (**b**) Depth profile of volumetric rates of anoxygenic photosynthesis, as derived from the light–dark shift method adapted for S_{tot}. For both panels, total sulphide concentrations, S_{tot}, were calculated from the measured H_2S concentrations and pH, and the incident irradiance during the light measurements was 100 µmol photons m^{-2} s^{-1}.

DCMU (data not shown), suggesting that obligate anoxygenic phototrophs were not significantly contributing to the light-driven sulphide consumption in the cyanobacterial layer. This was confirmed by the observation that exposure to near infrared light, which specifically targets bacteriochlorophylls of obligate anoxygenic phototrophs, did not induce sulphide consumption (Supplementary Figure S4).

Together these data show that the cyanobacterial community in the studied mats is able to perform oxygenic and sulphide-driven anoxygenic P simultaneously and that cyanobacterial anoxygenic P is fully responsible for the measured light-induced H_2S variation in the cyanobacterial layer of the mats.

Activity of C/B mats

Continuous *in situ* micro-profiling in C/B mats under naturally variable illumination gave consistent results with those obtained in the laboratory. In the dark, sulphide consumption rates were minute or

Table 1 Physico-chemical parameters in the overlying water column and in the studied mats

Mat type	*Site*	*H_2S (S_{tot}[a]) (µM)*[b]			*O_2 (µM)*[b]	*DIC (mM)*[c,d]	*pH*[b]	*NH_4^+ (µM)*[c,d]	*NO_x (µM)*[c, d]	*PAR*[e] *(µmol photons m^{-2} s^{-1})*	*T (°C)*
		W[f]	*C*[f]	*SOB*[f]							
C/B-1	Main Spring	73 (582)	345 (2755)	510 (3339)	0	4.2 (±0.18)	8.0	77 (±3.3)	34.4 (±1.9)	133	14
C/B-2	Main Spring	23 (151)	36 (287)	36 (353)	5	3.9 (±0.6)	8.0	56 (±4.7)	60 (±1.8)	93	14
C/B-3	Fissure Spring	401 (628)	415 (642)	435 (681)	5	8.9	6.9	150	<1	78	14.5
B/C-1	Main Spring	89 (278)	125 (390)	95 (175)	45	4.4 (± .15)	7.5	206 (±10.2)	3.6 (±0.07)	124	13
B/C-2	Main Spring	50 (92)	81 (149)	73 (88)	65	4.7 (±0.11)	7.3	–	–	163	13
B/C-3	Fissure Spring	16 (248)	61	34	80	–	8.3	<1	50	–	15

Abbreviations: DIC, dissolved inorganic carbon; PAR, photosynthetically available radiation; SOB, sulphur-oxidizing bacteria.
[a]Total sulfide concentration, S_{tot}, was calculated from the measured H_2S concentration and pH.
[b]Values are derived from microsensor measurements performed during night. The values obtained during the day are shown in Supplementary Table S2.
[c]Values were determined from water samples taken during night. The values determined from samples taken during the day are shown in Supplementary Table S2.
[d]Values in parentheses refer to s.d. ($n = 3$–6).
[e]Downwelling irradiance of the PAR, given as the average photon flux during 15 h of light.
[f]Concentrations in the water column (W) inside the cyanobacterial layer (C) and the layer dominated by large SOB, as derived from microsensor measurements.

below detection limit, as implied by essentially flat S_{tot} profiles across the mats during the night, and O_2 was not detected (Supplementary Figure S3). At sunrise, while still at low light, the rate of sulphide removal owing to anoxygenic P in the cyanobacterial layer sharply increased, resulting in a gradual decrease in H_2S concentrations (Figure 4a). Around midday, when the incident irradiance exceeded about 300 µmol photons $m^{-2} s^{-1}$, sulphide concentrations within the cyanobacterial layer decreased and the photosynthetic production of oxygen sharply increased (Figure 4a). These dynamics occurred essentially in reverse order at sunset.

In situ measurements under controlled light conditions revealed additional insights into the activity of C/B mats. At high incident irradiance (650 µmol photons $m^{-2} s^{-1}$), the cyanobacterial community performed both oxygenic and anoxygenic P simultaneously, as shown by the light–dark shift measurements (Figure 5b). Aerobic respiration in the photosynthetically active zone was negligible, as the net diffusive flux of oxygen from the zone was very similar to the gross rates of oxygenic P depth-integrated over the zone (2.43 and 2.47 µmol $m^{-2} s^{-1}$, respectively). Although oxygenic P was detectable at depths 0–0.6 mm, anoxygenic P was detectable only at depths 0–0.4 mm, that is, in zones of the cyanobacterial layer where both H_2S and light were abundant. The overlap between the zone of anoxygenic photosynthetic activity and the decrease in S_{tot} from the overlying water indicated that the sulphide used by the cyanobacteria originated exclusively from the overlying water. This was supported by the close match between the depth-integrated rates of gross anoxygenic P (1.56 µmol S_{tot} $m^{-2} s^{-1}$) and the downward S_{tot} flux from the water column (1.55 µmol S_{tot} $m^{-2} s^{-1}$) (Figures 5a and b). When oxygenic P was, however, not active (that is, in the morning and later in the afternoon), the flux of S_{tot} consumed by anoxygenic P had significant contributions from both the downward and upward components of the diffusive S_{tot} flux.

Sulphide consumption in the SOB layer was detectable only after the onset of oxygenic P by the cyanobacteria (Figures 4b and 5a). This observation is consistent with the absence of an external supply of an electron acceptor, that is, O_2, from the water column and additionally indicates that anaerobic sulphide oxidation with NO_3^- as the electron acceptor was not important. Once O_2 became available, sulphide consumed by the SOB originated exclusively from below, while the sulphide entering the mat from above was consumed by the cyanobacteria (see above).

Analysis of the profiles in Figure 5a revealed that the photosynthetically produced O_2 (downward flux 0.85 µmol O_2 $m^{-2} s^{-1}$) and the sulphide supplied from below (upward flux 0.48 µmol S_{tot} $m^{-2} s^{-1}$) were consumed at a S_{tot}/O_2 flux ratio of about 0.6. However, a detailed analysis of the complete sets of profiles measured in the C/B mat over a diel cycle (Supplementary Figure S3) revealed that the S_{tot}/O_2

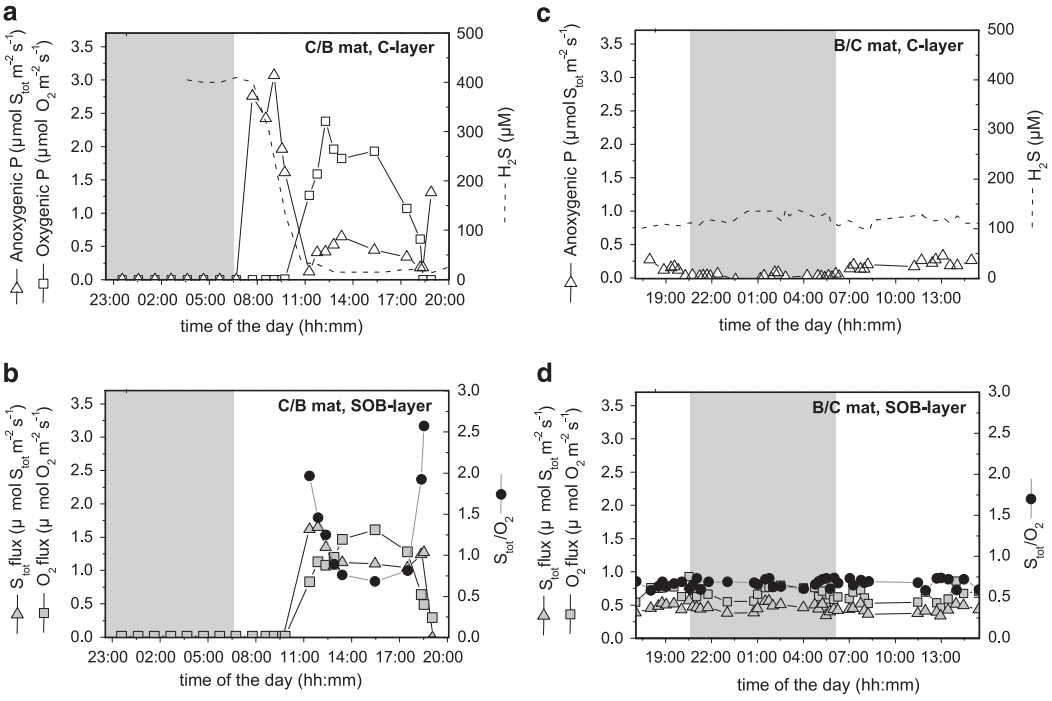

Figure 4 Activity of the cyanobacterial (**a** and **c**) and SOB (**b** and **d**) populations in the C/B (**a** and **b**) and B/C (**c** and **d**) mats exposed to natural light fluctuations over a 24-h period. The fluxes were derived from *in situ* microsensor profiles of O_2 and H_2S concentration (Supplementary Figures S5 and S6) and pH. The corresponding average H_2S concentration in the cyanobacterial layer, and the S_{tot}/O_2 flux ratio in the SOB layer, are also shown. Open and shaded areas correspond to light and dark, respectively.

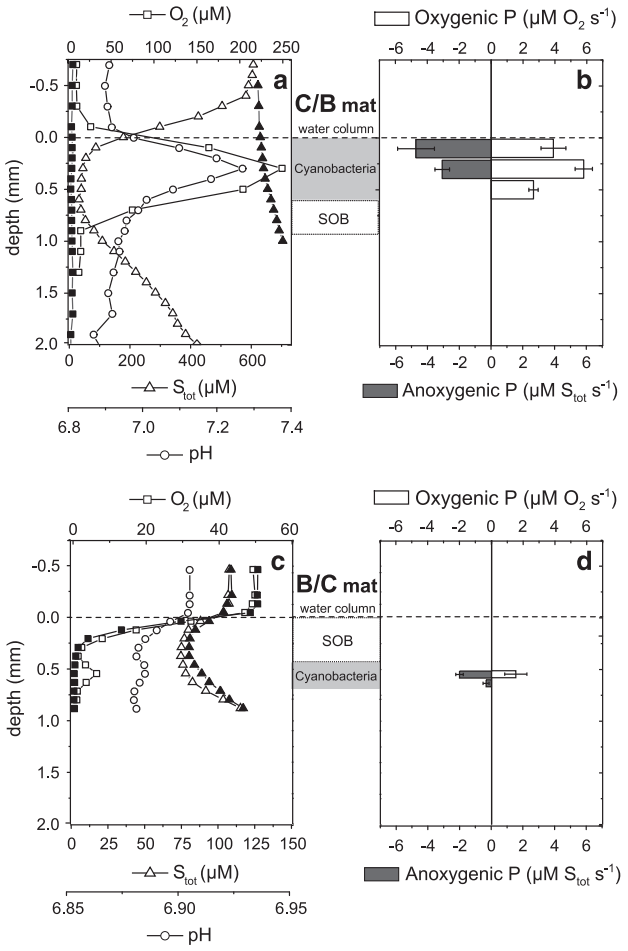

Figure 5 Microsensor measurements in the C/B and B/C mats under artificially controlled light conditions. Measurements in the C/B (**a** and **b**) and B/C mats (**c** and **d**) were performed *in situ* and *ex situ*, respectively. Left panels show steady-state depth profiles of O_2, S_{tot} and pH in the light (open symbols) and in the dark (closed symbols). Right panels show the corresponding depth profiles of volumetric rates of oxygenic and anoxygenic photosynthesis, as derived from light–dark shift microsensor measurements of O_2 and S_{tot}, respectively. For all panels, total sulphide concentrations, S_{tot}, were calculated from the measured H_2S concentrations (not shown) and pH. The incident irradiance during the light measurements in the C/B and B/C mats was 650 and 710 μmol photons $m^{-2} s^{-1}$, respectively. For orientation, approximate structures of the mats are also shown.

consumption ratio changed substantially over the course of the day, reaching about 2 after O_2 became available, gradually decreasing to about 0.7 before increasing back to about 2.6 just before O_2 depletion towards the night (Figure 4b). Similar patterns in the diurnal variations of the S_{tot}/O_2 consumption ratio between 0.7 and 2.6 were also observed in a replicate C/B mat (Supplementary Figures S5A and B).

The observed diurnal variation in the S_{tot}/O_2 consumption ratio in the SO zone can be explained by assuming that the SOB activity varied between incomplete oxidation of sulphide to S^0 and complete oxidation of sulphide to SO_4^{2-} when the S_{tot}/O_2 ratio reached the maximum and minimum value, respectively. This assumption made it possible to estimate the energy conservation efficiency of the SOB community. Specifically, using the maximum value of $S_{tot}/O_2 = 2.6$ (oxidation to S^0) and additionally taking into account the measured local concentrations of the substrates and products involved, we found the efficiency values of 16.6% and 16.5% for the two replicate C/B mats. Conversely, the minimum value of $S_{tot}/O_2 = 0.7$ (complete oxidation to SO_4^{2-}) measured in the respective mats gave the efficiency values of 17.2% and 17.1% (calculation details given in Supplementary Information 2.2). These calculations suggest that the energy conservation efficiency of the SOB community in the studied mats was around 16.9% and did not significantly depend on the S^0/SO_4^{2-} production ratio.

The S_{tot}/O_2 consumption ratio in both replicate C/B mats was significantly negatively correlated with the downward O_2 flux from the cyanobacterial layer ($R^2 = 0.91$, $P < 0.0001$), as well as with the local concentration of O_2 ($R^2 = 0.91$, $P < 0.0001$) and H_2S ($R^2 = 0.66$, $P = 0.008$), but not correlated with the upward S_{tot} flux ($R^2 = 0.27$, $P = 0.15$; Supplementary Figure S6). In one of the C/B mats, the availability of sulphide from below was low and thus the minimum S_{tot}/O_2 consumption ratio of 0.7, which indicates complete oxidation of sulphide to sulphate (see above), was reached early during the day (Supplementary Figure S5B). When this ratio was reached, we observed a pronounced downward shift of the zone where sulphide was aerobically consumed (Supplementary Figure S5C). This downward shift did not affect the correlation between the S_{tot}/O_2 consumption ratio and the O_2 flux or the local O_2 and H_2S concentrations.

Taken together, our data suggest that in the layer underneath the photic zone aerobic sulphide oxidation by SOB was the only significant sink of oxygen in the layer while aerobic heterotrophic activity was negligible. Therefore, we conclude that the SOB population in the C/B mats most likely varied its activity between incomplete and complete aerobic sulphide oxidation to S^0 and SO_4^{2-}, respectively (that is, at a variable S^0/SO_4^{2-} production ratio), whereby this variability was regulated by the availability of O_2 produced locally by the overlying cyanobacteria and by the local H_2S concentration but not by the flux of sulphide from below.

Activity of B/C mats

Despite the fact that B/C mats were exposed to similarly high incident light intensities as the C/B mats (Table 1), sulphide removal in these mats owing to anoxygenic P was not very pronounced (Figure 4c). Also oxygenic P was very low or even below detection limit in the B/C mats (Figure 4c; Supplementary Figure S7). This was confirmed by *ex situ* measurements under controlled light conditions. Specifically, the depth-integrated rates of gross anoxygenic and oxygenic P were about one order of magnitude lower than in C/B mats at similar irradiances and remained low even when the applied

irradiance exceeded the maximal values measured *in situ* (Figure 5d; Supplementary Figure S7). Additionally, the rate of O_2 consumption in the cyanobacterial layer (such as by aerobic respiration), calculated as the difference between the gross and net rates of O_2 produced in the layer (Figures 5c and d), was not significant in the B/C mats. Also, the depth-integrated rates of gross anoxygenic P (0.20 μmol $S_{tot}\,m^{-2}\,s^{-1}$) matched closely the net S_{tot} flux (0.19 μmol $S_{tot}\,m^{-2}\,s^{-1}$) consumed in the cyanobacterial layer, indicating that anoxygenic P was the only significant sink of sulphide in this layer. The source of this photosynthetically removed sulphide was exclusively from below.

Sulphur and oxygen cycling in B/C mats was dominated by the light-independent aerobic chemolithotrophic SO in the top SOB layer (Figures 4d and 5c). In the dark, sulphide for aerobic SO originated from both the water column and the underlying sediment. During high light conditions, the downward sulphide flux from the water column was the main source, while the upward sulphide flux was mostly consumed in the cyanobacterial layer (see above; Figure 5c). Additionally, during the maximum incident irradiance, consumption of O_2 produced locally by the underlying cyanobacterial layer only contributed <15% to the overall O_2 consumption in the SOB layer. Thus SO in the top layer relied mostly on O_2 supplied externally from the overlying water column.

Over the course of the day, the S_{tot}/O_2 consumption ratio remained constant at about 0.67 (Figure 4d). Thus aerobic SO by the SOB community in the B/C mats was in steady state and therefore most likely proceeded completely to sulphate (Nelson *et al.*, 1986; Jørgensen *et al.*, 2010). Using this stoichiometry, we estimated the energy conservation efficiency of the SOB community in the two replicate B/C mats to be 16.4% and 17.1% (calculation details given in Supplementary Information 2.2), which is very similar to the value estimated for the SOB community in the C/B mats (see above).

Light absorption by the cyanobacteria

C/B and B/C mats back-reflected 4.5% and 81% of the incident irradiance, respectively. This suggests that the estimated fractions of the incident flux of light energy absorbed by the cyanobacterial populations were 95.5% and 19%, respectively (see Supplementary Information 1). However, these values likely define the upper limits of the light energy utilized by cyanobacteria in the mats, as light absorption could occur also owing to abiotic components in the mats (Al-Najjar *et al.*, 2012).

Carbon and energy budgets

Assuming that photosynthesis by cyanobacteria and aerobic sulphide oxidation by SOB were the only processes responsible for oxygen and sulphide cycling, we used the measured fluxes of light, oxygen and sulphide together with the estimated energy conservation efficiency of the SOB populations to estimate daily carbon and energy budgets in the two studied mat types (Table 2). The C/B mats conserved about 2.42% of the incident light energy directly by P (split into 1.83% by oxygenic and 0.59% by anoxygenic P). This conservation efficiency was increased to about 2.54% when additionally considering that the photosynthetically produced oxygen is used for SOB-driven carbon fixation coupled to aerobic chemosynthetic SO. When expressed in terms of fixed carbon, the exploitation of the thermodynamic disequilibrium between O_2 and sulphide, which was internally generated by oxygenic P, thus increased the total primary productivity in the C/B mats by 15% (from 67.5 to 79.5 mmol $C\,m^{-2}\,d^{-1}$).

In contrast, the B/C mats conserved only about 0.12% of the incident light energy by P (mainly by anoxygenic P), although the daily flux of light energy available for both mat types was similar. Instead, energy conservation in the B/C mats was dominated by chemosynthesis (about 69% of the total energy conserved), although the daily flux of light energy available to the system was about 67-fold larger than the flux of chemical energy (in the form of oxygen and sulphide diffusing from the water column, utilized by aerobic SO). Thus, because of the small contribution of P, the overall energy conversion efficiency in the B/C mats was only 0.37%, that is, sevenfold lower than in the C/B mats. This grossly inefficient utilization of the available light energy in the B/C mats is also reflected in the estimated overall primary productivity, which was about threefold lower than in the C/B mats (23.4 vs 79.5 mmol $C\,m^{-2}\,d^{-1}$; Table 2). Analysis of the replicate measurements led to similar conclusions although with slightly different numerical values (Supplementary Table S2).

Discussion

The dominant functional groups in the Frasassi spring mats, photosynthetic cyanobacteria and aerobic chemolithoautotrophic SOB are directly coupled as both oxygen and sulphide are involved in their energy-generation pathways. The two functional groups, however, depend on different energy sources, that is, on light and chemical energy, respectively. Our results show that activity in the mats is driven by both energy sources. However, depending on the direction and temporal dynamics of the energy supply, the mats stratified in essentially two distinct structures, C/B mats and B/C mats, characterized by substantially different activity patterns and, most strikingly, utilization efficiencies of the externally available energy.

C/B mats

In C/B mats, cyanobacteria inhabiting the photic layer switched between anoxygenic and oxygenic

Table 2 Daily budgets of compounds and energy utilized by photosynthesis (P, anoxygenic and oxygenic) and by aerobic sulphide oxidation (SO) in the two end-member mat types

	C/B mat			*B/C mat*		
	P (anoxyP; oxyP)	*SO*	*Total (P; SO)*	*P (anoxyP; oxyP)*	*SO*	*Total (P; SO)*
O_2 flux[a] (mmol $O_2\,m^{-2}\,d^{-1}$)	43.93	−34.11	9.82	0.0	−56.30	−56.30
S_{tot} flux[a] (mmol $S_{tot}\,m^{-2}\,d^{-1}$)	−47.12	−32.28	−79.34	−8.63	−37.67	−46.30
CO_2 flux[a] (mmol $CO_2\,m^{-2}\,d^{-1}$)	−67.49 (34.9%; 65.1%)	−12.04	−79.53 (84.9%; 15.1%)	−4.32 (100%; 0%)	−19.06	−23.38 (18.5%; 81.5%)
Energy flux available[b] (kJ $m^{-2}\,d^{-1}$)	1572.53	13.22[c]	1585.75 (99.2%; 0.8%)	1455.74	21.68	1477.34 (98.5%; 1.5%)
Energy flux conserved (kJ $m^{-2}\,d^{-1}$)	38.10 (24.4%; 75.6%)	2.24	40.34 (94.5%; 5.5%)	1.70 (100%; 0%)	3.71	5.41 (31.43%; 68.6%)
Conservation efficiency[d]	2.42% (0.59%; 1.83%)	16.9%	**2.54%** (2.40%; 0.14%)	0.12% (0.12%; 0)	17.1%	**0.37%** (0.12%; 0.25%)

[a]Positive and negative values are used when the compound is produced and consumed, respectively.
[b]Energy gained by aerobic SO was assumed to represent also the energy available for this process.
[c]Represents energy generated internally within the ecosystem as a consequence of oxygenic P.
[d]Calculated as energy conserved divided by energy available. The total energy conservation efficiency of the mats is highlighted in bold.

P over a diurnal cycle, with microzones performing oxygenic and anoxygenic P simultaneously (Figures 4 and 5). As C/B mats formed in areas characterized by a very low O_2 concentration (<5 μM) in the overlying water (Table 1), oxygenic P was the exclusive provider of electron acceptor for aerobic SO.

Because of the fluctuating availability of light, the supply of oxygen to the SOB population residing under the cyanobacterial population was also fluctuating. A possible adaptation of SOB to live under such conditions is to rapidly adjust their SO stoichiometry, that is, to vary the S^0/SO_4^{2-} product ratio, depending on the availability of O_2 and S_{tot}, whereby the range of S_{tot}/O_2 consumption rations that can be covered by the SOB through the variation between the complete and incomplete oxidation of sulphide to sulphate and zero-valent sulphur, respectively, is determined by the corresponding energy-conservation efficiency (Klatt and Polerecky, 2015). Our data suggest that this strategy was adopted by the SOB in the C/B mats. Specifically, we estimated that the dominant SOB performed aerobic SO with an energy conservation efficiency of ~16.9%, which allowed them to adjust their S_{tot}/O_2 consumption ratio to the range of S_{tot}/O_2 flux ratios imposed by the environment (between ~0.7 and ~2.6) and thus harvest the available fluxes of sulphide and oxygen optimally.

Interestingly, when the S_{tot}/O_2 consumption ratio reached the minimum value of 0.7, that is, when sulphide oxidation proceeded entirely to sulphate, a further increase in the rate of oxygen supply by oxygenic P led to a downward migration of the SOB. We suggest that this is because the SOB could not adjust the S_{tot}/O_2 consumption ratio below the minimum value determined by their energy conservation efficiency (Klatt and Polerecky, 2015), leaving the adjustment of their position as the only option to maintain optimal utilization of the available substrates in the dynamically changing gradients of sulphide and O_2. There are two plausible hypotheses concerning the exact trigger for migration: (i) the biomass-dependent maximum rate of O_2 consumption was reached, or (ii) the rate of O_2 consumption by the SOB became limited by the supply of H_2S. In both cases, any further increase in oxygenic P would lead to an increase in the local O_2 concentration triggering downward migration owing to a phobic response to O_2 (Møller *et al.*, 1985).

Intriguingly, the S_{tot}/O_2 consumption ratio was only determined by the O_2 flux and the local H_2S concentration but not by the S_{tot} flux (Supplementary Figure S6). This is consistent with the expectation that SOB should adjust their S^0/SO_4^{2-} production ratio so as to maximize utilization of the available O_2. This is because the carbon yield per oxygen is expected to be almost constant irrespective of the S^0/SO_4^{2-} production ratio, that is, the O_2 reduction rate directly translates into growth, as suggested by the fact that the energy-conversion efficiencies estimated for the incomplete and complete SO in

the SOB inhabiting the C/B mats were almost equal (Klatt and Polerecky, 2015).

Together, the flexible O_2-dependent adjustment of the S^0/SO_4^{2-} production ratio seems to allow the SOB to efficiently exploit the chemical energy in the system and to additionally build up storage of intracellular S^0 that might serve as an electron acceptor for anaerobic respiration during night when the O_2 is not available (Schwedt *et al*., 2011). The dominant SOB therefore appear to be highly adapted to co-exist with oxygenic phototrophs.

Overall, under the oxygen-limited conditions in C/B mats, both photosynthetic and aerobic chemosynthetic activity are regulated by light energy supplied to the system. Despite the dependence of both anoxygenic P and chemolithotrophy on H_2S as an electron donor, its light-dependent depletion was not disadvantageous for the SOB because the chemolithotrophic and phototrophic layers did not compete for the same sulphide pool. Specifically, chemolithotrophic activity was exclusively supplied by the sulphide flux from below while the photosynthetically oxidized sulphide originated from the overlying water column. Aerobic SO by SOB, or for that matter any aerobic activity, was directly coupled to both oxygenic and anoxygenic P, the latter required to locally deplete the reductant (H_2S) so as to enable the former. Therefore, both anoxygenic and oxygenic photosynthetic activities were beneficial for the SOB, as they together allowed for the life-enabling production of oxygen required for the SOB to thrive under the particular oxygen-limiting conditions where C/B mats developed.

B/C mats

In B/C mats, SOB formed a layer on top of the cyanobacteria, where they could access a continuous supply of energy (H_2S and O_2) from the water column throughout the entire diel cycle (Figure 4d). In contrast, the energy source (light) for the cyanobacteria in the B/C mats was discontinuous. We hypothesize that the continuity of the energy supply was the main advantage that the SOB had over cyanobacteria in the B/C mats. Specifically, in the absence of light during the night the cyanobacteria were not triggered to assert themselves in the uppermost position of the mat, that is, closest to the energy sources for both functional groups during the day. This has been taken advantage of by the SOB, whose chemolithotrophic activity in this position could continue uninterrupted. During the day the position of the cyanobacteria remained in the lower part of the mat, where the light availability was significantly reduced (at least fivefold) owing to intense back-scattering in the overlying layer of SOB (Supplementary Information 1). Therefore, the cyanobacteria were not able to harvest the light optimally. It remains unclear how exactly the very distinct layering was maintained during the day and why the cyanobacteria were not able to invade the SOB layer. An important factor was probably faster motility of the SOB that made them more successful competitors for the 'prime spot' on top of the mats.

Importance of energy flux direction and dynamics for mat structure and function

When oxygen provided externally from the water column was limiting, light availability regulated the activity and spatial organization of the dominant functional groups, leading to the formation of C/B mats. In these mats, primary productivity was exclusively driven by light. Namely, light energy was directly utilized by anoxygenic and oxygenic P and indirectly facilitated productivity of the SOB that exploited the chemical energy in the form of the thermodynamic disequilibrium driven by photosynthetically produced O_2. Consequently, processes stratified predictably according to the direction and magnitude of the energy source, and the dominant functional groups, photosynthetic cyanobacteria and aerobic SOB, beneficially interacted. This led to an efficient utilization of the available external energy.

B/C mats, on the other hand, were exposed to two energy sources, both of which had the same direction, that is, they were externally supplied from the water column, and were therefore most abundant at the upper surface of the mat. One of these sources, namely, chemical energy in the form of oxygen and sulphide, was continuous, while the other, light, was diurnally fluctuating. As the functional groups competed for the space closest to their energy sources, specific adaptation mechanisms (for example, motility) and phenotypic features (for example, light-scattering S^0 globules) gained in importance. Intriguingly, the organisms specialized in utilizing chemical energy, SOB, outcompeted all photosynthetic microbes from the position closest to the light, even though the availability of light energy per day was orders of magnitude higher than that of chemical energy. This means that the continuously available chemical energy was used preferentially, while the additional potential for gaining oxygen via internal recycling of the other available external energy source (light) was neglected or even suppressed. As a consequence, the competition for a favourable position in the mat led to a comparatively inefficient use of the bulk external energy.

It is also likely that nitrogen retention, storage and removal in the two mat types strongly differ owing to the differences in the O_2 concentrations in the water column overlying the C/B and B/C mats and the differences in the activity of the SOB and cyanobacteria in the mats. To understand possible effects of this on the mat stratification, more detailed measurements of bioavailable nitrogen in the mats would be required, which could, however, not be done during this study owing to technical limitations. Nevertheless, the lack of correlation between the mat type and the water column concentrations of NO_3^- and NH_4^+ (Table 1) suggests that nitrogen cycling is an

unlikely factor that determines the formation of a certain mat type.

Implications

The scenario in C/B mats resembles what is thought to have been the arena for the evolutionary transition from anoxygenic to oxygenic P in the ancient phototrophic microbial mats in isolated shallow water environments. The environment where these critical steps in evolution occurred was chemically reduced (for example, Tice and Lowe, 2004; Sessions *et al.*, 2009; Lyons *et al.*, 2014). Anoxygenic P using the available reductants, for example, H_2S, is expected to be an important process in such environments. However, H_2S can become locally depleted, which provides a selective advantage to cyanobacteria that are able to switch from anoxygenic to oxygenic P (Cohen *et al.*, 1986; Jørgensen *et al.*, 1986; Klatt *et al.*, 2015) and that are therefore never limited by electron donors. In C/B mats, this versatility leads to the introduction of aerobic hotspots in the otherwise reduced environment.

The C/B mats also demonstrate the revolutionary consequences of creating such aerobic hotspots. Oxygen as the most favourable electron acceptor offers a myriad of thermodynamic strategies for other microorganisms, and oxygenic P has therefore set the basis for the co-evolution of aerobic organisms. Initially, as the proliferation of oxygenic P and aerobic metabolisms took place in otherwise anoxic and reduced environments, these two processes were spatially and temporarily closely coupled. This is illustrated in C/B mats, where aerobic SO was completely dependent on the internal conversion of light energy into chemical energy driven by the photosynthetic production of oxygen.

Despite the substantial consumption of oxygen by aerobic chemolithotrophy in the layer underneath the photic zone, C/B mats were net sources of oxygen to the water column. It is assumed that, in ancient, more reduced oceans, excess reductants have initially scavenged the photosynthetically produced oxygen, and it was only upon depletion of these sinks that oxygen could persistently accumulate in the atmosphere and upper water column of the oceans during the Great Oxidation Event. However, the Great Oxidation Event was possibly predated by transient accumulations of oxygen in the atmosphere (the 'whiffs of oxygen') (for example, Anbar *et al.*, 2007; Lyons *et al.*, 2014), and it is not unlikely that, despite reductant availability, oxygen had also persistently accumulated in the shallow water column above microbial mats, similarly to the scenario in the Frasassi sulphidic springs. Independent of the exact timing, water column oxygenation freed aerobic organisms from consortia and microenvironments where O_2 was provided exclusively through the close proximity to oxygenic phototrophs (that is, oxygen oases; for example, Buick, 2008). A paradoxical consequence of this is strikingly demonstrated in the Frasassi B/C mats. Although these mats were exposed to light and contained significant populations of oxygenic phototrophs, they became a net sink for oxygen once it accumulated in the water column. This is because they were mainly driven by an aerobic, light-independent process (SO). This demonstrates that an aerobic metabolism, which had, by necessity, evolved dependent on light, could even outcompete the oxygenic phototrophs that formerly served as the exclusive provider of oxygen for its energy metabolism.

The oxygenation of the Earth's atmosphere represents an event where oxygen has evolved from a fluctuating internal source of chemical energy into a continuous external source. We suggest that aerobic chemosynthesis might have become competitive against photosynthesis, thus tempering photosynthesis-driven primary productivity and providing a negative feedback on the proliferation of oxygenic phototrophic organisms. As demonstrated by the Frasassi mats, the effect of this negative feedback could have been as radical as a turn from a hugely productive ecosystem that acts as a net O_2 source (C/B mat) into a considerably less productive ecosystem that acts as a net O_2 sink (B/C mat). Further research is required to identify possible biosignatures of this competitive interaction between phototrophs and aerobic chemolitotrophs that could be searched for in geological records to explore whether the negative-feedback hypothesis could be generalized beyond the highly localized scale of this study.

Conflict of Interest

The authors declare no conflict of interest.

Acknowledgements

We thank Daniel S Jones (University of Minnesota) for invaluable help in the field, Alessandro Montanari and Paula Metallo for providing laboratory facilities and enjoyable atmosphere at the Osservatorio Geologico di Coldigioco and Tim Ferdelman for fruitful discussions. We thank the technicians of the microsensor group for microsensor construction. This work was financially supported by the Max Planck Society, by a 2011 'For Women in Science Award' to JMK and by NASA Astrobiology Institute (PSARC, NNA04CC06A) and Hanse-Wissenschaftskolleg Fellowship funds to JLM.

References

Al-Najjar MAA, de Beer D, Jørgensen BB, Kühl M, Polerecky L. (2010). Conversion and conservation of light energy in a photosynthetic microbial mat ecosystem. *ISME J* **4**: 440–449.

Al-Najjar MAA, de Beer D, Kühl M, Polerecky L. (2012). Light utilization efficiency in photosynthetic microbial mats. *Environ Microbiol* **14**: 982–992.

Allwood AC, Grotzinger JP, Knoll AH, Burch IW, Anderson MS, Coleman ML *et al.* (2009). Controls on development and diversity of Early Archean stromatolites. *Proc Natl Acad Sci USA* **106**: 9548–9555.

Anbar AD, Duan Y, Lyons TW, Arnold GL, Kendall B, Creaser RA *et al.* (2007). A whiff of oxygen before the great oxidation event? *Science* **317**: 1903–1906.

Berg P, Risgaard-Petersen N, Rysgaard S. (1998). Interpretation of measured concentration profiles in sediment pore water. *Limnol Oceanogr* **43**: 1500–1510.

Braman RS, Hendrix SA. (1989). Nanogram nitrite and nitrate determination in environmental and biological materials by vanadium(III) reduction with chemiluminescence detection. *Anal Chem* **61**: 2715–2718.

Buick R. (2008). When did oxygenic photosynthesis evolve? *Philos Trans R Soc Lond B Biol Sci* **363**: 2731–2743.

Castresana J, Saraste M. (1995). Evolution of energetic metabolism: the respiration-early hypothesis. *Trends Biochem Sci* **20**: 443–448.

Catling DC, Glein CR, Zahnle KJ, McKay CP. (2005). Why O2 is required by complex life on habitable planets and the concept of planetary 'oxygenation time'. *Astrobiology* **5**: 415–438.

Cline JD. (1969). Oxygenation of hydrogen sulfide in seawater at constant salinity, temperature and pH. *Environ Sci Technol* **3**: 838–843.

Cohen Y, Jørgensen BB, Revsbech NP, Poplawski R. (1986). Adaptation to hydrogen sulfide of oxygenic and anoxygenic photosynthesis among cyanobacteria. *Appl Environ Microbiol* **51**: 398–407.

de Beer D, Schramm A, Santegoeds CM, Kühl M. (1997). A nitrite microsensor for profiling environmental biofilms. *Appl Environ Microbiol* **63**: 973–977.

Dismukes GC, Klimov V V, Baranov S V, Kozlov YN, DasGupta J, Tyryshkin A. (2001). The origin of atmospheric oxygen on Earth: the innovation of oxygenic photosynthesis. *Proc Natl Acad Sci USA* **98**: 2170–2175.

Galdenzi S, Cocchioni M, Morichetti L, Amici V, Scuri S. (2008). Sulfidic ground-water chemistry in the Frasassi Caves, Italy. *J Cave Karst Stud* **70**: 94–107.

Grotzinger JP, Knoll AH. (1999). Stromatolites in Precambrian carbonates: evolutionary mileposts or environmental dipsticks? *Annu Rev Earth Planet Sci* **27**: 313–358.

Hall POJ, Aller RC. (1992). Rapid, small-volume, flow injection analysis for ∑(CO2) and NH4+ in marine and freshwaters. *Limnol Oceanogr* **37**: 1113–1119.

Jeroschewski P, Steuckart C, Kühl M. (1996). An amperometric microsensor for the determination of H2S in aquatic environments. *Anal Chem* **68**: 4351–4357.

Jørgensen BB, Cohen Y, Revsbech NP. (1986). Transition from anoxygenic to oxygenic photosynthesis in a *Microcoleus chthonoplastes* cyanobacterial mat. *Appl Environ Microbiol* **51**: 408–417.

Jørgensen BB, Dunker R, Grünke S, Røy H. (2010). Filamentous sulfur bacteria, Beggiatoa spp., in arctic marine sediments (Svalbard, 79 degrees N). *FEMS Microbiol Ecol* **73**: 500–513.

Klatt JM, Al-Najjar MAA, Yilmaz P, Lavik G, de Beer D, Polerecky L. (2015). Anoxygenic photosynthesis controls oxygenic photosynthesis in a cyanobacterium from a sulfidic spring. *Appl Environ Microbiol AEM* **81**: 2025–2031.

Klatt JM, Polerecky L. (2015). Assessment of the stoichiometry and efficiency of CO2 fixation coupled to reduced sulfur oxidation. *Front Microbiol* **6**: 484.

Lassen C, Ploug H, Jørgensen BB. (1992). A fibre-optic scalar irradiance microsensor: application for spectral light measurements in sediments. *FEMS Microbiol Lett* **86**: 247–254.

Lyons TW, Reinhard CT, Planavsky NJ. (2014). The rise of oxygen in Earth's early ocean and atmosphere. *Nature* **506**: 307–315.

Millero F. (1986). The thermodynamics and kinetics of the hydrogen sulfide system in natural waters. *Mar Chem* **18**: 121–147.

Møller MM, Nielsen LP, Jørgensen BB. (1985). Oxygen responses and mat formation by Beggiatoa spp. *Appl Environ Microbiol* **50**: 373–382.

Nelson DC, Jørgensen BB, Revsbech NP. (1986). Growth pattern and yield of a chemoautotrophic Beggiatoa sp. in oxygen-sulfide microgradients. *Appl Environ Microbiol* **52**: 225–233.

Polerecky L, Bachar A, Schoon R, Grinstein M, Jørgensen BB, de Beer D *et al.* (2007). Contribution of Chloroflexus respiration to oxygen cycling in a hypersaline microbial mat from Lake Chiprana, Spain. *Environ Microbiol* **9**: 2007–2024.

Polerecky L, Bissett A, Al-Najjar MAA, Färber P, Osmers H, Suci PA *et al.* (2009). Modular spectral imaging system for discrimination of pigments in cells and microbial communities. *Appl Environ Microbiol* **75**: 758–771.

Revsbech NP, Jørgensen BB. (1983). Photosynthesis of benthic microflora measured with high spatial resolution by the oxygen microprofile method: capabilities and limitations of the method. *Limnol Oceanogr* **28**: 749–759.

Revsbech NP. (1989). An oxygen microsensor with a guard cathode. *Limnol Oceanogr* **34**: 474–478.

Schopf J. (2012). The fossil record of Cyanobacteria. In: Whitton BA (ed). *Ecology of Cyanobacteria II*. Springer: Dordrecht, Netherlands, pp 15–36.

Schwedt A, Kreutzmann A-C, Polerecky L, Schulz-Vogt HN. (2011). Sulfur respiration in a marine chemolithoautotrophic Beggiatoa strain. *Front Microbiol* **2**: 276.

Seckbach J, Oren A (eds). (2010). *Microbial Mats: Modern and Ancient Microorganisms in Stratified Systems*. Springer: Dordrecht, Netherlands.

Sessions AL, Doughty DM, Welander PV, Summons RE, Newman DK. (2009). The continuing puzzle of the great oxidation event. *Curr Biol* **19**: R567–R574.

Sherwood JE, Stagnitti F, Kokkinn MJ, Williams WD. (1991). Dissolved oxygen concentrations in hypersaline waters. *Limnol Oceanogr* **36**: 235–250.

Tice MM, Lowe DR. (2004). Photosynthetic microbial mats in the 3,416-Myr-old ocean. *Nature* **431**: 549–552.

Van der Meer MTJ, Schouten S, Bateson MM, Nübel U, Wieland A, Kühl M *et al.* (2005). Diel variations in carbon metabolism by green nonsulfur-like bacteria in alkaline siliceous hot spring microbial mats from Yellowstone National Park. *Appl Environ Microbiol* **71**: 3978–3986.

Van Gemerden H, Mas J. (1995). Ecology of phototrophic sulfur bacteria. In: Blankenship RE, Madigan MT, Bauer CE (eds). *Anoxygenic Photosynthetic Bacteria, Advances in Photosynthesis and Respiration*, Vol. 2. Springer Netherlands: Dordrecht, The Netherlands, pp 49–85.

Ward DM, Bauld J, Castenholz RW, Pierson BK. (1992). Modern phototrophic microbial mats: anoxygenic,

intermittently oxygenic/anoxygenic, thermal, eukaryotic, and terrestrial. In: Schopf JW, Klein C (eds). *The Proterozoic Biosphere: A Multidisciplinary Study*. Cambridge University Press: NY, USA, pp 309–324.

Weber M, Färber P, Meyer V, Lott C, Eickert G, Fabricius KE *et al*. (2007). In situ applications of a new diver-operated motorized microsensor profiler. *Environ Sci Technol* **41**: 6210–6215.

Wieland A, Kühl M. (2000). Short-term temperature effects on oxygen and sulfide cycling in a hypersaline cyanobacterial mat (Solar Lake, Egypt). *Mar Ecol Prog Ser* **196**: 87–102.

Supplementary Information accompanies this paper on The ISME Journal website (http://www.nature.com/ismej)

Structure and function of natural sulphide oxidizing microbial mats under dynamic input of light and chemical energy

Klatt, J. M.; Meyer, S.; Häusler, S.; Macalady, J.L.; de Beer, D.; Polerecky, L.

Supplementary Information

Content

1. Absorption of light energy by the cyanobacterial population in the studied microbial mats

2. Conversion of fluxes of O_2, S_{tot} and light to fluxes of fixed CO_2 and conserved energy

   2.1. Photosynthesis (P)

   2.2. Aerobic chemolithoautotrophic sulphide oxidation (SO)

3. Supplementary Figures

4. Supplementary Tables

5. Supplementary References

1. Absorption of light energy by the cyanobacterial population in the studied microbial mats

Reflectance of the C/B mats and B/C, denoted as $R_{C/B}$ and $R_{B/C}$, respectively, was measured as previously described (Al-Najjar *et al.*, 2010), using a fibre-optic field radiance microsensor (Jørgensen & Marais, 1988; Kühl & Jørgensen, 1994). To arrive at expressions for the fraction of the incident light energy absorbed by the cyanobacterial population in the mat, A_C, we modeled light propagation in the two mat types as schematically shown in Figure S8.

For the C/B mats we assumed that light attenuation occurred only due to absorption by cyanobacteria (Figure S8A). Thus we calculated A_C as $1 - R_{C/B}$.

In the B/C mats the light path and its interaction with the microorganisms were more complicated and therefore A_C was estimated as follows. First, we assumed that light attenuation in the top layer dominated by large sulphur oxidizing bacteria (SOB) occurred only due to scattering. Second, approximating the B/C mat by a two-layer optical structure, we assumed that propagation of the incident light energy flux, I_0, through the mat followed boundary conditions summarized in Figure S8B. Specifically, at the upper interface of the SOB layer, the upwelling light flux was a sum of the component that was back-scattered from the SOB layer, $I_0 R_B$, and the component that was twice transmitted through the SOB layer and once back-scattered from the cyanobacterial layer, $I_0 T_B^2 R_C$. Consequently, the reflectance of the B/C mat, defined as the ratio between the upwelling and downwelling light fluxes, was approximated as

$$R_{B/C} = R_B + R_C T_B^{\,2} . \qquad (1)$$

The assumption of no light absorption in the SOB layer implied that $R_B = 1 - T_B$, which made it possible to rewrite Eq. 1 as a quadratic equation for T_B,

$$0 = R_C T_B^{\,2} - T_B + (1 - R_{B/C}) , \qquad (2)$$

from which T_B can be calculated as

$$T_B = \frac{1 \pm \sqrt{1 - 4R_C(1 - R_{B/C})}}{2R_C} . \qquad (3)$$

In this equation, only the expression with the '–' sign was considered as physically meaningful, because the one with the '+' sign yielded $T_B > 1$.

Following Figure S8B, A_C in the B/C mats is given by

$$A_C = T_B(1 - R_C) , \qquad (4)$$

which accounts for the fact that the light absorbed (i.e., not back-scattered) by the cyanobacteria (factor $1 - R_C$) must have been first transmitted through the SOB layer (factor T_B).

Because it was not possible to determine the reflectance of the cyanobacterial layer in the B/C mat without destroying the mat, we assumed that it was equal to the experimentally determined

reflectance of the cyanobacteria in the C/B mat, i.e., $R_C = R_{C/B}$. Combining Eqs. 3 and 4, A_C in the B/C mat was therefore estimated as

$$A_C = \frac{(1 - R_{C/B})\left(1 - \sqrt{1 - 4R_{C/B}(1 - R_{B/C})}\right)}{2R_{C/B}}. \quad (5)$$

Experimentally determined reflectance values were $R_{C/B}$ = 0.045 and $R_{B/C}$ = 0.81, which implied A_C = 0.955 for the C/B mat and A_C = 0.183 for the B/C mat. Since the cyanobacterial layer in the B/C mats was thinner and less dense than in the C/B mats, R_C was most likely lower than $R_{C/B}$. Furthermore, some light absorption probably occurred also in the SOB layer. Thus, the fraction of incident light energy absorbed by cyanobacteria in the B/C mats was probably lower than the upper limit of 0.183.

2. Conversion of fluxes of O_2, S_{tot} and light to fluxes of fixed CO_2 and conserved energy

Here we provide the details of how we estimated the fluxes of CO_2 fixed and energy conserved by the two dominant processes in the studied mats – photosynthesis and aerobic sulphide oxidation – from the measured fluxes of O_2 and S_{tot}. We assumed that the conserved energy comprises two components: (i) energy required for the reduction of the electron carrier (e.g., $NADP^+$) that is used as the electron donor for the reduction of CO_2, and (ii) energy required in the actual CO_2 fixation pathway.

2.1. *Photosynthesis (P)*

Photosynthetic CO_2 fixation by cyanobacteria was assumed to follow reactions

$$H_2O + CO_2 \rightarrow O_2 + CH_2O, \quad (6)$$

$$2\ H_2S + CO_2 \rightarrow 2\ S^0 + CH_2O + H_2O, \quad (7)$$

where the first and second reaction corresponds to oxygenic and anoxygenic P, respectively. We assumed H_2S (not HS^-) to be the substrate for, and elemental sulphur (S^0) to be the product of, anoxygenic P (Cohen *et al*., 1986; Arieli *et al*., 1991; Griesbeck *et al*., 2000; Klatt *et al*., 2015).

To quantify the **net flux of C fixed by oxygenic P** ($J_{C,oxy\text{-}P}$, in mol C m^{-2} s^{-1}), we used the measured O_2 flux in combination with the CO_2/O_2 stoichiometry of 1, i.e.,

$$J_{C,oxy\text{-}P} = J_{O2,oxy\text{-}P}. \quad (8)$$

Here, $J_{O2,oxy\text{-}P}$ (in mol O_2 m^{-2} s^{-1}) is the sum of the upward and downward diffusive fluxes from the cyanobacterial layer into the water-column and into the SOB layer, respectively, derived from *in situ* microsensor profiles. Analogously, to quantify the **net flux of C fixed by anoxygenic P** ($J_{C,anoxy\text{-}P}$, in mol C m^{-2} s^{-1}), we used the measured S_{tot} flux together with the CO_2/S_{tot} stoichiometry of 1/2, i.e.,

$$J_{C,anoxy\text{-}P} = 0.5\ J_{Stot,,anoxy\text{-}P} \quad (9)$$

Here, $J_{Stot,,anoxy\text{-}P}$ (in mol S_{tot} m^{-2} s^{-1}) is the total sulphide flux consumed in the cyanobacterial layer, as derived from *in situ* microsensor profiles.

To quantify the **flux of energy conserved by oxygenic P** ($J_{E,oxy\text{-}P}$, in kJ m^{-2} s^{-1}), we multiplied the CO_2 flux with the energy demand of oxygenic P, i.e.,

$$J_{E,oxy\text{-}P} = \Delta E_r(\text{oxy-P})\ J_{C,oxy\text{-}P}. \quad (10)$$

Here, the energy demand ΔE_r(oxy-P) was calculated by considering that during oxygenic P two separate energy-demanding reactions are performed. Specifically, CO_2 reduction in the Calvin cycle requires conversion of ATP into ADP and P_i. Assuming an ATP energy content of 41 kJ $(\text{mol ATP})^{-1}$, the energy requirement of the Calvin cycle is $\Delta G_r(CO_2\ \text{fix}) = 123$ kJ $(\text{mol } CO_2)^{-1}$ (Supplemental material of Bar-Even et al., 2010). ATP is generated via the light energy-driven membrane-associated electron transport reactions. These reactions additionally have to provide two moles of reducing equivalents NADPH required for the reduction of one mole of CO_2. Using the Gibbs free energies of formation given by Thauer et al. (1977) and (Alberty, 1998) energy demand for $NADP^+$ reduction

coupled to H_2O oxidation is 533 kJ (2 mol $NADP^+)^{-1}$ = 533 kJ (mol $CO_2)^{-1}$. Thus, by summing up these two contributions we obtained ΔE_r(oxy-P) = 656 kJ (mol $CO_2)^{-1}$.

Analogously, we quantified the **flux of energy conserved by anoxygenic P** ($J_{E,anoxy\text{-}P}$, in kJ m^{-2} s^{-1}) by multiplying the energy demand of anoxygenic P with the CO_2 flux consumed by anoxygenic P ($J_{C,anoxy\text{-}P}$, in mol CO_2 m^{-2} s^{-1}), i.e.,

$$J_{E,anoxy\text{-}P} \text{ (kJ m}^{-2}\text{ s}^{-1}\text{)} = \Delta E_r\text{(anoxy-P)}\ J_{C,anoxy\text{-}P}. \quad (11)$$

Here, ΔE_r(anoxy-P) is the sum of the energy demand for $NADP^+$ reduction by H_2S (74 kJ (mol $CO_2)^{-1}$) and for CO_2 fixation (123 kJ (mol $CO_2)^{-1}$), i.e., ΔE_r(anoxy-P) = 197 kJ (mol $CO_2)^{-1}$.

2.2. *Aerobic chemolithoautotrophic sulphide oxidation (SO)*

Chemolithoautotrophic microorganisms derive their energy for CO_2 reduction from a chemical reaction with negative ΔG_r. For aerobic SO this reaction is H_2S oxidation with O_2. H_2S additionally serves as the electron donor for the reduction of CO_2. To calculate the fluxes of CO_2 fixed and energy gained and conserved by SO in the studied mats, we followed the generic theoretical framework described in Klatt & Polerecky (2015). According to this framework, the generalized equation for aerobic SO coupled to CO_2 reduction is

$$H_2S + y\,(2 - 1.5x)\,O_2 + (1 - y)\,(2 - 1.5x)\,CO_2 + (1 - y)\,(2 - 2.5x)\,H_2O \rightarrow$$
$$x\,S^0 + (1 - x)\,SO_4^{2-} + (1 - y)\,(2 - 1.5x)\,CH_2O + y\,x\,H_2O + (2 - 2x)\,H^+, \quad (12)$$

where x and $(1 - x)$ describe the fractions of the sulphide pool oxidized to S^0 and SO_4^{2-}, respectively, and y and $(1 - y)$ describe the fractions of the sulphide pool used for energy generation and CO_2 reduction, respectively (both x and y are between 0 and 1).

To calculate the **flux of CO_2 fixed by aerobic SO**, we note that the stoichiometric coefficients for S_{tot}, O_2 and CO_2 in Eq. 12 are related as

$$\frac{S_{tot}}{O_2} = \frac{1}{y(2-1.5x)} \quad (13)$$

and

$$\frac{CO_2}{O_2} = \frac{1-y}{y}, \quad (14)$$

Thus, if the parameter x is known, Eq. 13 makes it possible to calculate the parameter y from the measured ratio of the S_{tot} and O_2 fluxes consumed by aerobic SO, which can subsequently be used to calculate the flux of CO_2 fixed ($J_{C,SO}$, in mol C m^{-2} s^{-1}) from the flux of O_2 consumed ($J_{O2,SO}$, in mol O_2 m^{-2} s^{-1}) by aerobic SO from Eq. 15, namely as

$$J_{C,SO} = \frac{1-y}{y} J_{O2,SO}\ . \quad (15)$$

To calculate the flux of energy gained ($J_{E,SO,gained}$, in kJ m^{-2} s^{-1}) and conserved ($J_{E,SO}$, in kJ m^{-2} s^{-1}) by aerobic SO, we additionally took into account the efficiency of energy conservation by SO, denoted hereafter as ε. As described in Klatt and Polerecky (2015), this efficiency can be calculated once the parameters *x* and *y* are known using the function `aerob_efficiency` available at http://nanosims.geo.uu.nl/SOX. Thus, the **flux of energy conserved by aerobic SO** was calculated as

$$J_{E,SO} = (1 - y)\, \Delta G_r(\mathrm{SO, CO_2\ red})\, J_{Stot,SO}, \quad (16)$$

where $J_{Stot,SO}$ is the flux of S_{tot} consumed by aerobic SO (in mol S_{tot} m^{-2} s^{-1}) and ΔG_r(SO, CO_2 red) is the energy required for the reduction of CO_2 in aerobic SO (in kJ (mol H_2S)$^{-1}$). This energy requirement was calculated as the sum of the energy needed to reduce NAD^+ in the reverse electron transport reaction and of the energy needed to fix CO_2 in the Calvin cycle (see Supplementary Figure S1 in Klatt & Polerecky, 2015). Finally, the **flux of energy gained by aerobic SO** to fuel CO_2 fixation was calculated as

$$J_{E,SO,gained} = -J_{E,SO} / \varepsilon, \quad (17)$$

as follows from Eq. 30 in Klatt and Polerecky (2015).

In the B/C mats we observed that the S_{tot}/O_2 consumption ratio in the SOB layer was approximately constant during the diurnal cycle (Fig. 4D, Fig. S5). This suggested that aerobic SO in these mats was in a steady state, which made it possible to assume that sulphide was oxidized completely to SO_4^{2-} (Jørgensen *et al.*, 2010). Using Eqs. 12–13, this implied that $x = 0$ and $y = [2(S_{tot}/O_2)]^{-1}$. For the two replicate B/C mats, the averaged values of the S_{tot}/O_2 consumption ratio measured in the SOB layer were 0.669 and 0.654 (Table S3), which translates into $y = 0.747$ and $y = 0.765$, respectively. Using these values together with the local H_2S and O_2 concentrations and pH measured *in situ* with microsensors (averaged over the SOB layer), and additionally assuming that the local sulphate concentrations (2 mM) and temperature (13–15 °C) in the SOB layer were the same as in the water column (see Tables 1 and S1), we obtained the energy conversion efficiency values of 17.1% and 16.4% for the SOB populations in the respective replicate B/C mats (Tables 2 and S2). These values fall between the efficiencies previously calculated for *Beggiatoa* str. MS-81-6 (12.3%) and *Beggiatoa* str. MS-81-1c (32.5%) (Hagen & Nelson, 1997; Klatt & Polerecky, 2015). Using these values of *x*, *y* and ε, we calcualted the fluxes of CO_2 fixed, energy conserved and energy gained by aerobic SO from the measured fluxes of S_{tot} and O_2 consumed in the SOB layer of the respective B/C mat using Eqs. 14–17.

In contrast to B/C mats, the S_{tot}/O_2 consumption ratio in the SOB layer of C/B mats varied strongly over the diurnal cycle (Fig. 4B and S5B). We assumed that this was due to the variable end product of SO (S^0 versus SO_4^{2-}), as parameterized by *x* in Eq. 12. To estimate the fluxes of CO_2 and energy under this scenario, we assumed that the highest measured S_{tot}/O_2 consumption ratio occurred when sulphide was oxidized incompletely to S^0 (i.e., when $x = 1$), whereas the lowest measured S_{tot}/O_2 ratio corresponded to complete sulphide oxidation to SO_4^{2-} (i.e., $x = 0$) (see Eq. 13). Using the same

approach as described above, we calculated the energy conservation efficiency ε for the two extreme cases. Specifically, the highest S_{tot}/O_2 consumption ratios measured in the two replicate C/B mats were 2.574 and 2.577, which gave the efficiency values of 16.6% and 16.5%, respectively. In contrast, the lowest S_{tot}/O_2 consumption ratios were 0.685 and 0.681, which gave the efficiency values of 17.2% and 17.1% in the respective mats. This striking similarity of the calculated values suggested that the SOB population in the studied mats performed aerobic SO with an efficiency that was independent of the end product (i.e., of the S^0/SO_4^{2-} ratio). In our subsequent calculations we assumed that this efficiency was equal to the average of the calculated values, i.e., 16.9%.

Therefore, to calculate the fluxes of CO_2 fixed, energy gained and energy conserved by aerobic SO in the SOB layer of the C/B mats, we first used the O_2 or S_{tot} concentration profiles determined *in situ* with microsensors to determine in every time-point (i) the average concentrations of H_2S and O_2 and pH in the overlapping zone of H_2S and O_2 and (ii) the fluxes of S_{tot} and O_2 consumed in this zone. Subsequently, we used Eq. 13 together with the average energy conservation efficiency of 16.9% and the S_{tot}/O_2 flux ratio to determine the values of *x* and *y* in Eq. 12, which we finally used together with Eqs. 15–17 to calculate the fluxes of CO_2 fixed, energy gained and energy conserved by SO. Detailed results obtained for one of the replicate C/B mats are shown in Table S3. The final results integrated over 24 h for the first and second replicate C/B mat are summarized in Table 2 and Table S2, respectively (column SO).

3. Supplementary Tables

Table S1: Chemical parameters in the water column above the studied mats measured during day.

Mat type	Site	H_2S (S_{tot}[1]) [µM][2]	O_2 [µM][2]	DIC [mM][3,4]	pH[2]	NH_4^+ [µM][3,4]	NO_x [µM][3,4]	T [°C]
C/B-1	Main Spring	73 (582)	0	4.1 (+/-0.31)	8.0	79 (+/- 2.0)	33.4 (+/- 1.8)	14
C/B-2	Main Spring	13 (103)	864	3.2 (+/- 0.8)	8.0	52 (+/- 3.9)	50 (+/- 8.9)	14.5
C/B-3	Fissure Spring	401 (628)	5	-	6.9	-	-	14.5
B/C-1	Main Spring	89 (278)	45	3.9 (+/-0.22)	7.5	199 (+/-5.2)	3.6 (+/- 0.07)	13
B/C-2	Main Spring	50 (92)	65	4.6 (+/-0.09)	7.3	-	-	13
B/C-3	Fissure Spring	16 (248)	80	-	8.3	-	-	15.5

[1] Total sulfide concentration, S_{tot}, was calculated from the measured H_2S concentration and pH.
[2] Values are derived from microsensor measurements performed during the day. The corresponding measurements during night are shown in Table 1.
[3] Values were determined from water samples taken during the day. The corresponding values determined for the night are shown in Table 1.
[4] Values in parentheses refer to standard deviations (n = 3 – 6).

Table S2: Daily budgets of reactants and energy utilized by photosynthesis (P, anoxygenic and oxygenic) and aerobic sulphide oxidation (SO) in the studied mats. Shown are results for the second replicate of each mat type.

	C/B-2 mat			B/C-2 mat		
	P (anoxyP; oxyP)	SO	Total (P; SO)	P (anoxyP; oxyP)	SO	Total (P; SO)
O_2 flux[1] ($mmol\ O_2\ m^{-2}\ d^{-1}$)	36.05	-12.90	23.15	0.65	-39.06	-38.41
S_{tot} flux[1] ($mmol\ S_{tot}\ m^{-2}\ d^{-1}$)	-25.44	-14.38	-39.82	-9.29	-25.54	-34.84
CO_2 flux[1] ($mmol\ CO_2\ m^{-2}\ d^{-1}$)	-48.77 (26.1%; 73.9%)	-5.09	-53.86 (90.5%; 9.5%)	-5.30 (12.3%; 87.7%)	-12.02	-17.30 (30.6%; 69.4%)
Energy flux available[2] ($kJ\ m^{-2}\ d^{-1}$)	1087.5	5.56[3]	1093.06 (99.5%; 0.5%)	1914.44	14.94	1929.38 (99.2%; 0.8%)
Energy flux conserved ($kJ\ m^{-2}\ d^{-1}$)	28.66 (17.5%; 82.5%)	0.94	29.60 (96.8%; 3.2%)	2.26 (81.1%; 18.9%)	2.46	4.72 (47.9%; 52.1%)
Conservation efficiency[4]	2.64% (0.46%; 2.17%)	16.9%	**2.71%** (2.62%; 0.09%)	0.12% (0.10%; 0.02%)	16.4%	**0.24%** (0.12%; 0.13%)

[1] Positive and negative values are used when the compound is produced and consumed, respectively.
[2] Energy gained by aerobic sulphide oxidation (SO) was assumed to represent also the energy available for this process.
[3] Represents energy generated internally within the mat through oxygenic P.
[4]Calculated as energy conserved divided by energy available.

Table S3: Theoretical stoichiometry together with the values of energy gained and energy conserved by aerobic sulphide oxidation (SO) in the studied mats. Shown are results for two B/C mats and one C/B mat.

	Measured with microsensors						Calculated			Stoichiometry	Energy conserved		Energy gained	
Mat	$J_{Stot,SO}$[1]	$J_{O2,SO}$[1]	S_{tot}/O_2	O_2[2]	H_2S[2]	pH	x	y	$J_{C,SO}$[1]		ΔE_r(SO, CO_2 red)[3]	$J_{E,SO}$[4]	ΔG_r(SO, O_2 red)[3]	$J_{E,SO,gained}$[4]
B/C-1	37.67	56.3	0.669	95	73	7.1	0	0.747	19.06	$H_2S + 1.49\ O_2 + 0.51\ CO_2 + 0.51\ H_2O \rightarrow 1\ SO_4^{2-} + 0.51\ CH_2O + 2\ H^+$	389.14	3.71	-770.55	21.68
B/C-2	25.54	39.06	0.654	40	30	6.5	0	0.765	12.00	$H_2S + 1.53\ O_2 + 0.47\ CO_2 + 0.47\ H_2O \rightarrow 1\ SO_4^{2-} + 0.47\ CH_2O + 2\ H^+$	409.48	2.46	-764.72	14.94
C/B-1	0.83	1.62	1.96	50	30	8.1	0.887	0.760	0.133	$H_2S + 0.51\ O_2 + 0.16\ CO_2 \rightarrow 0.89\ S^0 + 0.11\ SO_4^{2-} + 0.16\ CH_2O + 0.73\ H_2O + 0.23\ H^+$	132.85	51.65	-248.94	306.49
	1.13	1.65	1.46	80	30	8.0	0.724	0.750	0.258	$H_2S + 0.69\ O_2 + 0.23\ CO_2 \rightarrow 0.72\ S^0 + 0.28\ SO_4^{2-} + 0.23\ CH_2O + 0.50\ H_2O + 0.55\ H^+$	175.41	72.36	-347.14	429.59
	1.08	1.35	1.25	135	20	8.0	0.618	0.746	0.294	$H_2S + 0.80\ O_2 + 0.27\ CO_2 \rightarrow 0.62\ S^0 + 0.38\ SO_4^{2-} + 0.27\ CH_2O + 0.35\ H_2O + 0.76\ H^+$	203.60	69.81	-411.22	414.14
	1.20	1.07	0.89	150	24	7.9	0.321	0.739	0.476	$H_2S + 1.12\ O_2 + 0.40\ CO_2 + 0.08\ H_2O \rightarrow 0.32\ S^0 + 0.68\ SO_4^{2-} + 0.40\ CH_2O + 1.36\ H^+$	281.70	78.67	-590.00	466.53
	1.47	1.12	0.76	180	24	7.9	0.143	0.735	0.696	$H_2S + 1.31\ O_2 + 0.47\ CO_2 + 0.33\ H_2O \rightarrow 0.14\ S^0 + 0.86\ SO_4^{2-} + 0.47\ CH_2O + 1.71\ H^+$	327.81	97.29	-697.75	574.39
	1.61	1.10	0.69	183	23	7.9	0.006	0.733	0.856	$H_2S + 1.46\ O_2 + 0.53\ CO_2 + 0.53\ H_2O \rightarrow 0.01\ S^0 + 0.99\ SO_4^{2-} + 0.53\ CH_2O + 1.99\ H^+$	363.38	107.02	-780.11	630.72
	1.28	1.04	0.81	120	25	7.9	0.220	0.737	0.562	$H_2S + 1.23\ O_2 + 0.44\ CO_2 + 0.22\ H_2O \rightarrow 0.22\ S^0 + 0.78\ SO_4^{2-} + 0.44\ CH_2O + 1.56\ H^+$	307.74	84.17	-649.86	498.10
	0.64	1.24	1.93	50	32	8.0	0.879	0.761	0.104	$H_2S + 0.52\ O_2 + 0.16\ CO_2 \rightarrow 0.88\ S^0 + 0.12\ SO_4^{2-} + 0.16\ CH_2O + 0.72\ H_2O + 0.24\ H^+$	135.67	40.21	-253.88	239.57
	0.49	1.27	2.57	10	32	8.1	1	0.776	0.055	$H_2S + 0.39\ O_2 + 0.11\ CO_2 \rightarrow S^0 + 0.11\ CH_2O + 0.89\ H_2O$	104.15	29.74	-179.70	176.27

[1] in mmol m^{-2} d^{-1} for the B/C mats and µmol m^{-2} s^{-1} for the C/B mat.
[2] Averaged over the SO layer, in µM.
[3] in kJ (mol H_2S)$^{-1}$
[4] in kJ m^{-2} d^{-1} for the B/C mats and mJ m^{-2} s^{-1} for the C/B mat.

4. Supplementary Figures

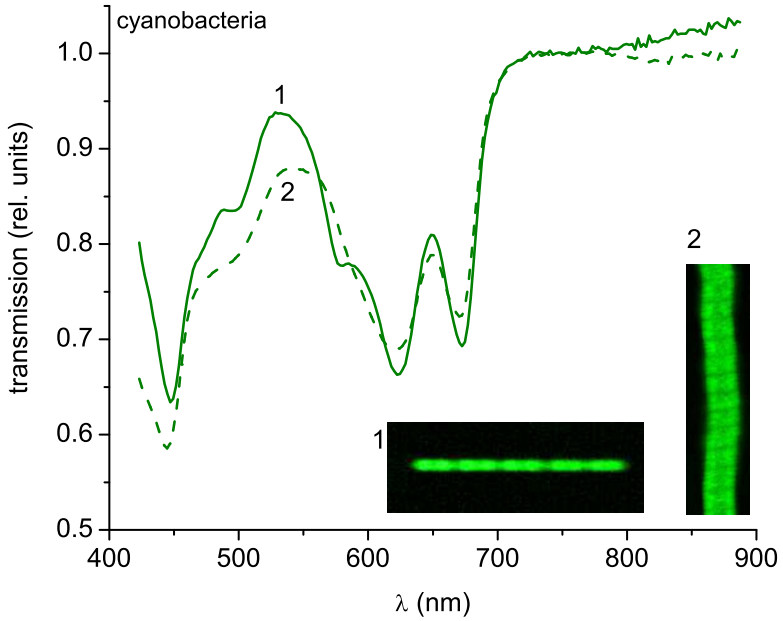

Figure S1: Hyperspectral imaging of two dominant cyanobacterial morphotypes found in the studied microbial mats. Shown are transmission spectra with clear spectroscopic signatures of cyanobacteria-specific pigments chlorophyll *a* (maximal *in vivo* absorption at wavelengths 680 nm and 450 nm) and phycocyanin (at 625 nm). Images of the filaments were constructed by assigning the curvature of the transmission spectrum at 680 nm to the intensity of the green channel (Polerecky *et al.*, 2009).

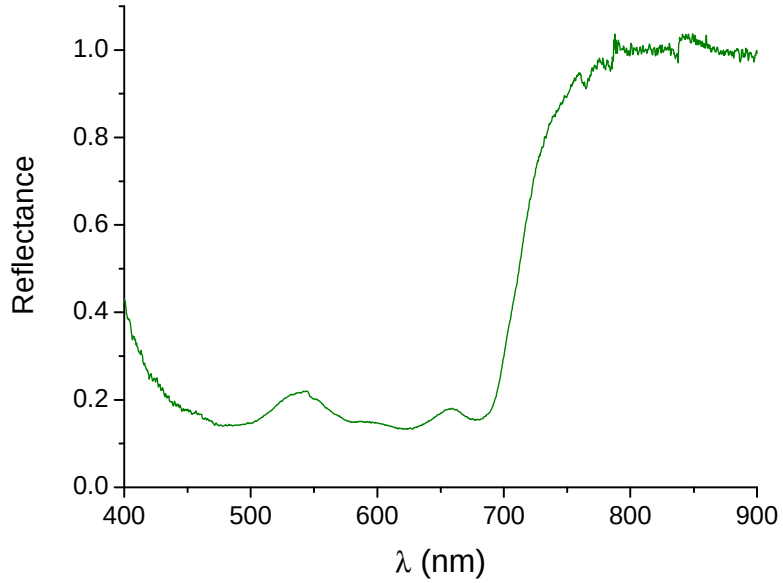

Figure S2: Example reflectance spectrum of a C/B mat. The spectrum shows spectroscopic signatures corresponding to cyanobacteria-specific pigments chlorophyll *a* and phycocyanin (maximal *in vivo* absorption at wavelengths 680 nm and 625 nm, respectively). The lack of spectral signatures of bacteriochlorophylls (absorption maxima between 700 and 890 nm; Polerecky *et al.* 2009) indicates that the abundance of obligatory anoxygenic phototrophs such as green or purple sulphur/non-sulphur bacteria in the studied mats was negligible.

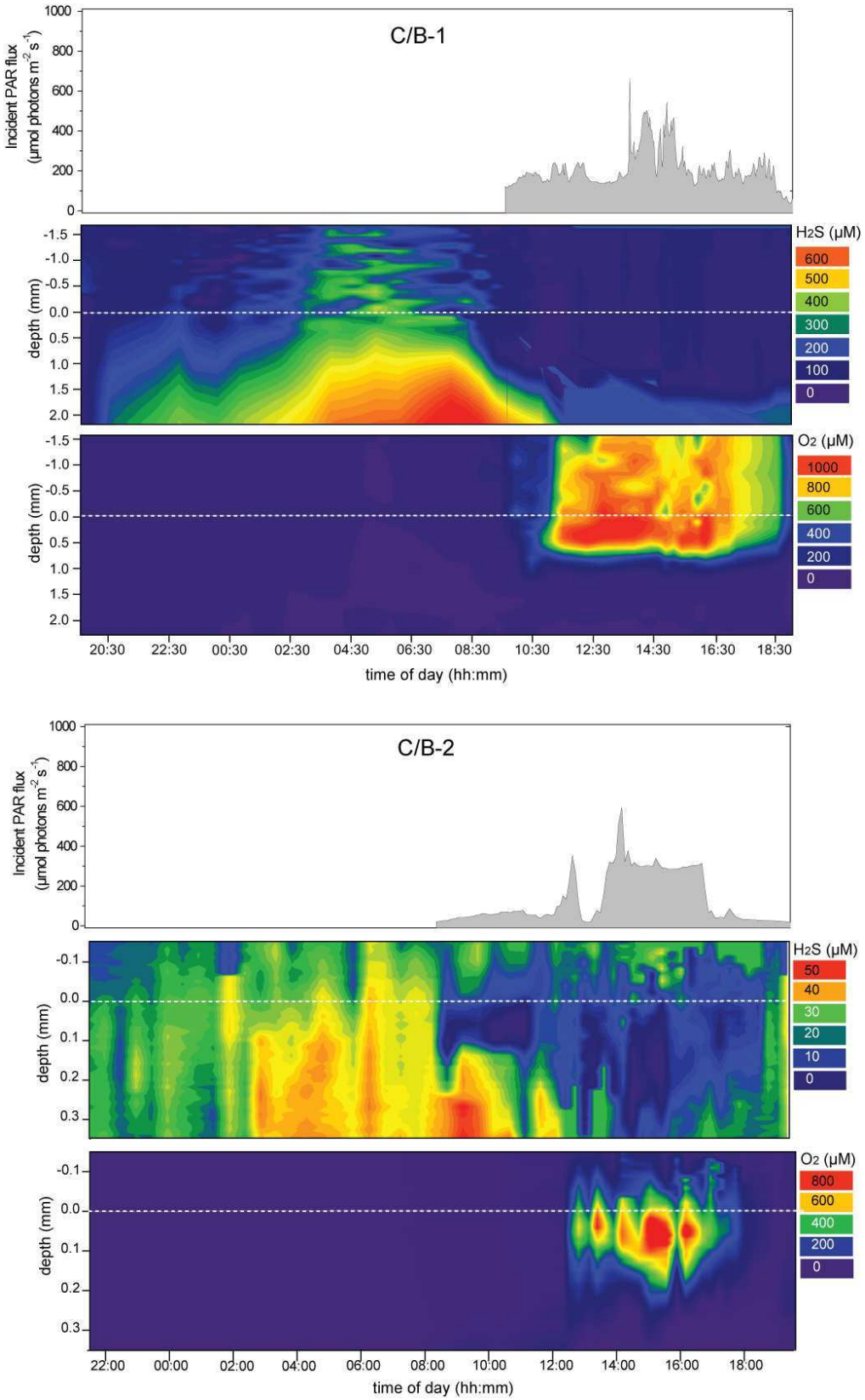

Figure S3: *In situ* measurements in the C/B mats over a 24 h period. Shown are downwelling irradiance of the photosynthetically available radiation (PAR) and vertical profiles of H_2S and O_2 concentrations as a function of time in two replicate mats. All measurements were done simultaneously, with microsensor tips separated by not more than 5 mm. Zero depth corresponds to the mat surface.

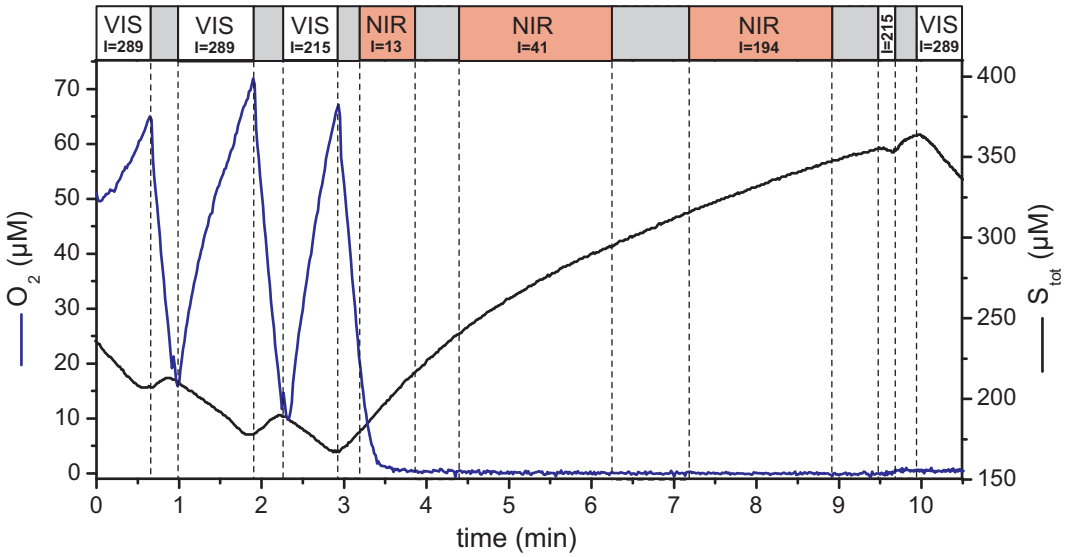

Figure S4: Light-induced dynamics of O_2, H_2S, S_{tot} and pH inside the cyanobacterial layer of a C/B mat. Total sulphide concentrations, S_{tot}, were calculated from the measured H_2S concentrations and pH. The irradiance was either in the visible (VIS; 400-700 nm) or near infrared (NIR; a mixture of light emitted by light-emitting diodes with emission maxima at 740 and 810 nm) part of the spectrum. Incident irradiance (I, in µmol photons m^{-2} s^{-1}) applied during the indicated time intervals is also shown (intervals shaded with gray correspond to darkness). Distance between sensor tips was < 5 mm.

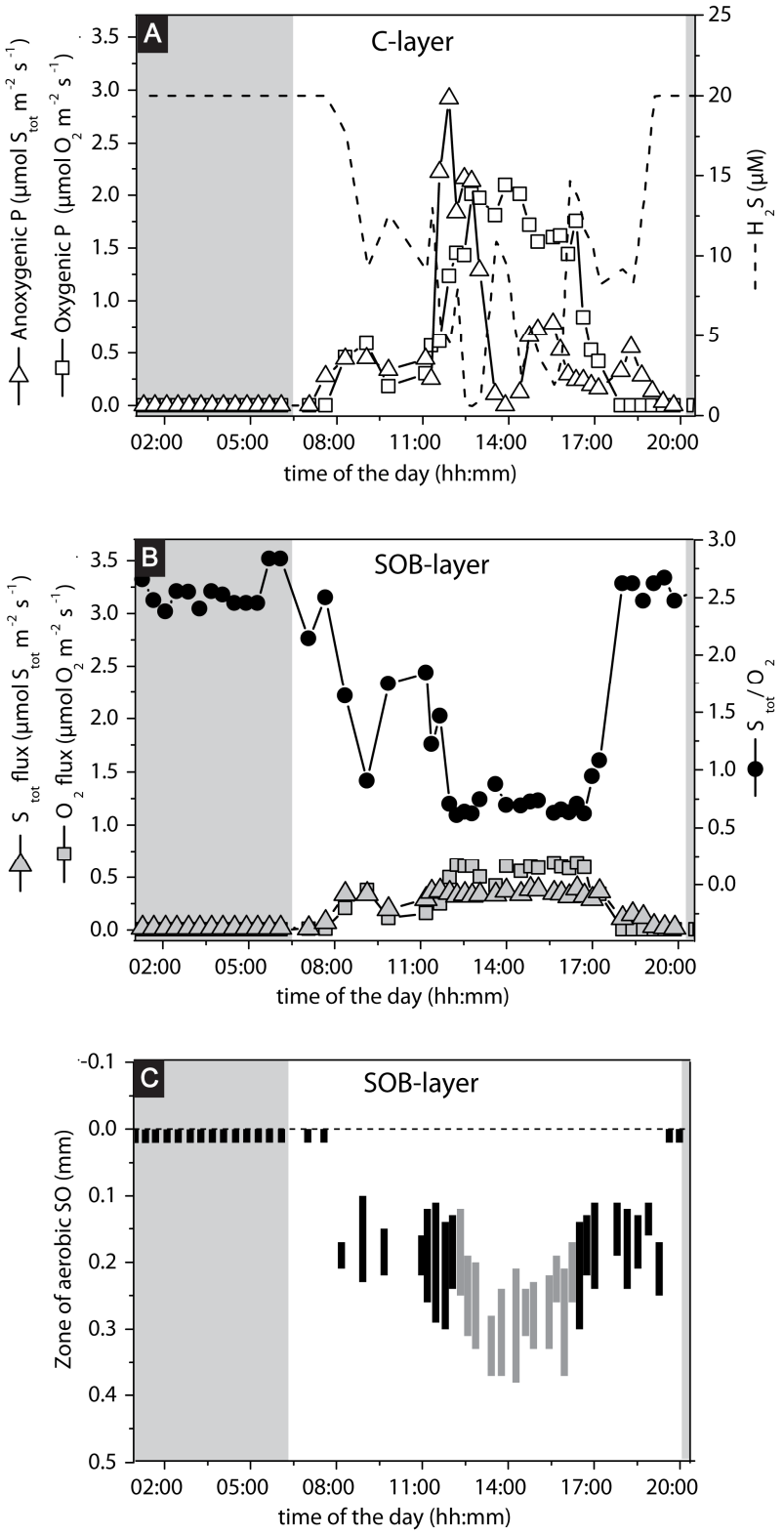

Figure S5: **Activity of cyanobacterial and SOB populations in the C/B-2 mat over a 24 h period.** The fluxes were derived from *in situ* microsensor profiles of O_2 and H_2S concentration (Fig. S3) and pH. The corresponding average H_2S concentration in the cyanobacterial layer, the S_{tot}/O_2 flux ratio in the SOB layer, and the depth interval of the zone in the mat where sulphide was oxidized with oxygen are also shown. Grey bars in panel C correspond to the time-points when the S_{tot}/O_2 consumption ratio was <0.7. In all panels shaded and non-shaded areas correspond to dark and light, respectively.

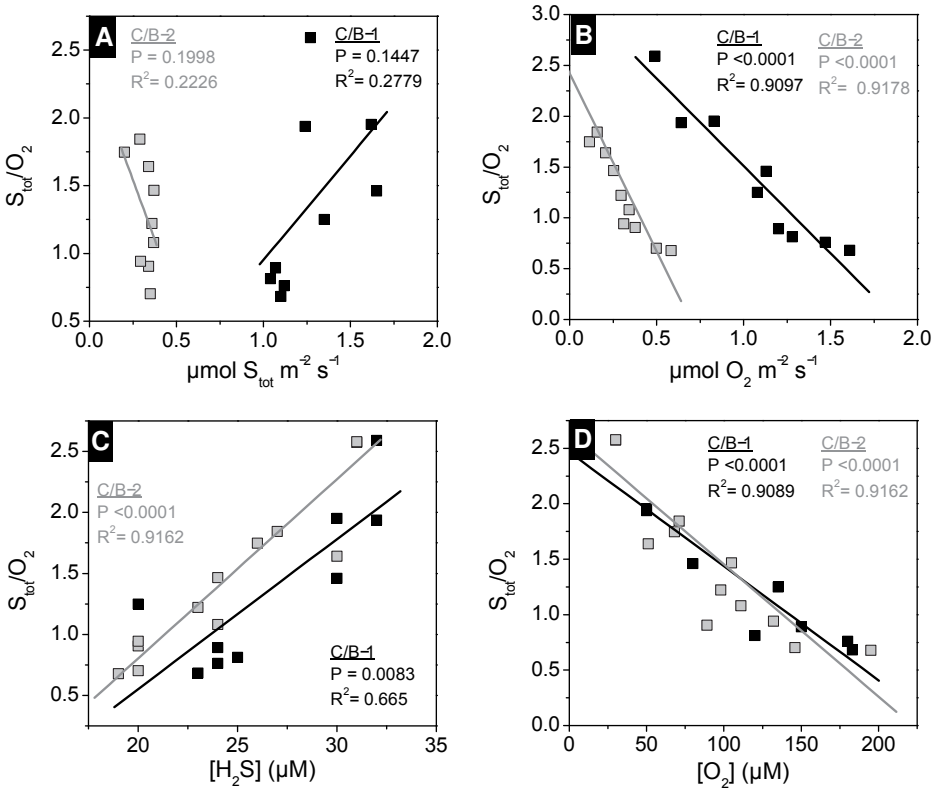

Figure S6: Regulation of aerobic SO in C/B mats. Shown are ratios between the fluxes of the total sulphide (S_{tot}) and O_2 consumed in the SOB layer (S_{tot}/O_2) as a function of the flux of S_{tot} consumed in the SOB layer (panel A), flux of O_2 consumed in the SOB layer (panel B), average concentration of H_2S in the SOB layer (panel C) and average concentration of O_2 in the SOB layer (panel D). All values were calculated from the concentration depth profiles measured *in situ*. Lines and legends show the results of the respective correlation analyses.

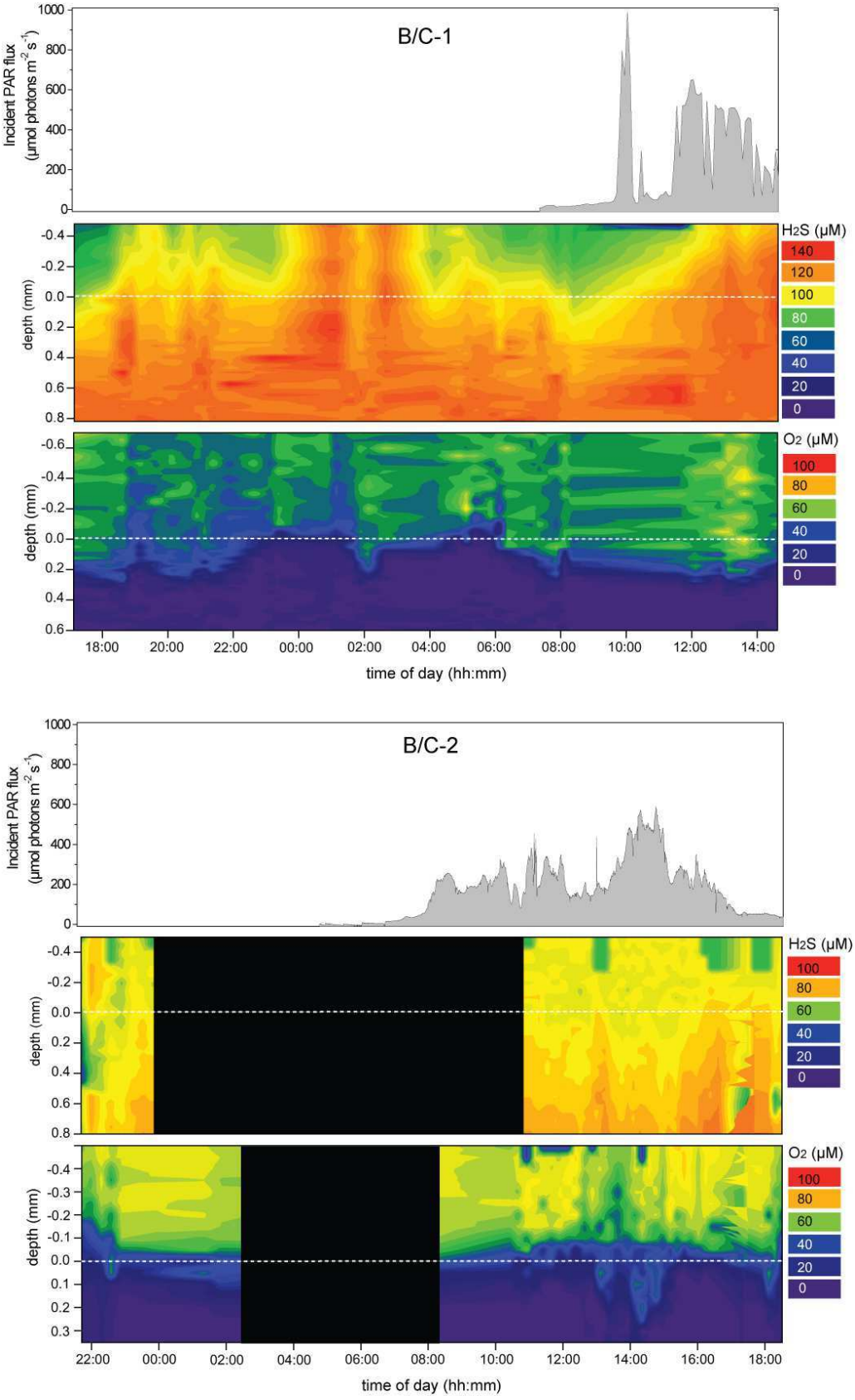

Figure S7: *In situ* measurements in the B/C mats over a 24 h period. Shown are downwelling irradiance of the photosynthetically available radiation (PAR), and vertical profiles of H_2S and O_2 concentrations as a function of time in two replicate mats. All measurements were done simultaneously, with microsensor tips separated by not more than 5 mm. Intervals when microsensor profiles were not recorded are shown in black. Zero depth corresponds to the mat surface.

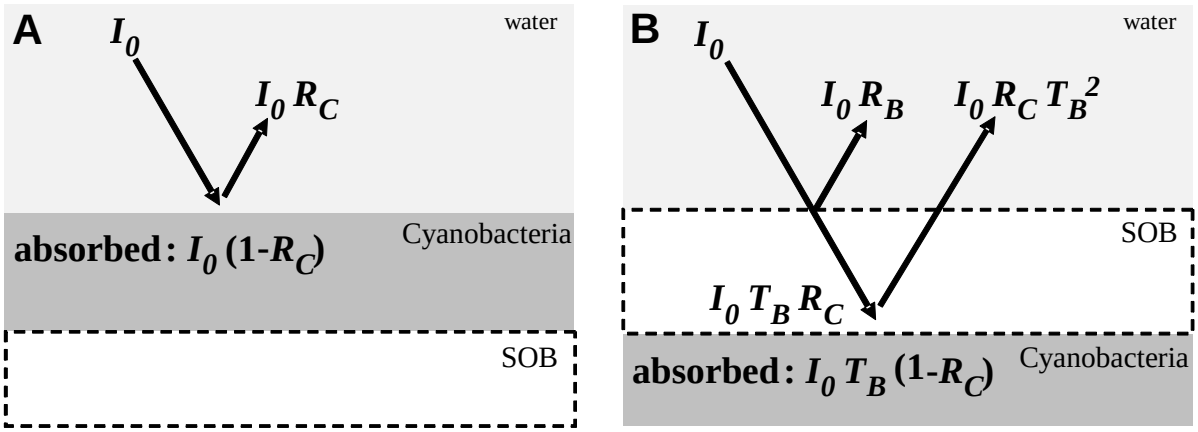

Figure S8: Schematic diagrams of the models of light propagation through a C/B and B/C mat. Shown are fluxes of incident, transmitted, absorbed and back-scattered ("reflected") light. Transmission and reflectance of the SOB layer is denoted by T_B and R_B, respectively, reflectance of the cyanobacterial layer as R_C, light energy flux as I_0.

5. Supplementary References

Alberty RA. (1998). Calculation of standard transformed formation properties of biochemical reactants and standard apparent reduction potentials of half reactions. *Arch Biochem Biophys* **358**:25–39.

Al-Najjar MAA, de Beer D, Jørgensen BB, Kühl M, Polerecky L. (2010). Conversion and conservation of light energy in a photosynthetic microbial mat ecosystem. *ISME J* **4**:440–449.

Arieli B, Padan E, Shahak Y. (1991). Sulfide-induced sulfide-quinone reductase activity in thylakoids of *Oscillatoria limnetica*. *J Biol Chem* **266**:104–11.

Bar-Even A, Noor E, Lewis NE, Milo R. (2010). Design and analysis of synthetic carbon fixation pathways. *Proc Natl Acad Sci U S A* **107**:8889–94.

Cohen Y, Jørgensen BB, Revsbech NP, Poplawski R. (1986). Adaptation to hydrogen sulfide of oxygenic and anoxygenic photosynthesis among cyanobacteria. *Appl Environ Microbiol* **51**:398–407.

Griesbeck C, Hauska G, Schütz M. (2000). Biological sulfide oxidation: Sulfide-quinone reductase (SQR), the primary reaction. *Recent Res Dev Microbiol* **4**:179–203.

Hagen KD, Nelson DC. (1997). Use of reduced sulfur compounds by *Beggiatoa* spp.: Enzymology and physiology of marine and freshwater strains in homogeneous and gradient cultures. *Appl Environ Microbiol* **63**:3957–3964.

Jørgensen BB, Dunker R, Grünke S, Røy H. (2010). Filamentous sulfur bacteria, *Beggiatoa* spp., in arctic marine sediments (Svalbard, 79 degrees N). *FEMS Microbiol Ecol* **73**:500–13.

Jørgensen BB, Marais DJ Des. (1988). Optical properties of benthic photosynthetic communities: fiber-optic studies of cyanobacterial mats. *Limnol Oceanogr* **33**:99–113.

Klatt JM, Al-Najjar MAA, Yilmaz P, Lavik G, de Beer D, Polerecky L. (2015). Anoxygenic photosynthesis controls oxygenic photosynthesis in a cyanobacterium from a sulfidic spring. *Appl Environ Microbiol* AEM.03579–14.

Klatt JM, Polerecky L. (2015). Assessment of the stoichiometry and efficiency of CO_2 fixation coupled to reduced sulfur oxidation. *Front Microbiol* **6**. doi:10.3389/fmicb.2015.00484.

Kühl M, Jørgensen BB. (1994). The light field of microbenthic communities: radiance distribution and microscale optics of sandy coastal sediments. *Limnol Oceanogr* **39**:1368–1398.

Polerecky L, Bissett A, Al-Najjar MAA, Färber P, Osmers H, Suci PA, *et al.* (2009). Modular spectral imaging system for discrimination of pigments in cells and microbial communities. *Appl Environ Microbiol* **75**:758–771.

Thauer RK, Jungermann K, Decker K. (1977). Energy conservation in chemotrophic anaerobic bacteria. *Bacteriol Rev* **41**:100–180.